April 2016

Design of a Novel Concept for Harnessing Tidal Stream Power: A Continuation

Andrea Yi Chan
Worcester Polytechnic Institute

Lauren Ann Richard
Worcester Polytechnic Institute

Nathan Gruebel Curtis
Worcester Polytechnic Institute

Sarah Melissa Bailey
Worcester Polytechnic Institute

Design of a Novel Concept for Harnessing Tidal Stream Power: A Continuation

A Major Qualifying Project submitted to the Faculty of Worcester Polytechnic Institute

In fulfillment of the requirements for the Degree of Bachelor of Science

Submitted by:

Sarah Bailey

Andrea Chan

Nathan Curtis

Lauren Richard

Authorship:

Sarah Bailey

Katrina Bradley

Andrea Chan

Nathan Curtis

Lauren Richard

Date:

28 April 2016

Project Advisor:

Brian Savilonis

Table of Contents

Table of Figures

Table of Tables

Abstract

The Water Energy Harvester MQP provides design insight into a novel system that collects energy from flowing water. This project is a continuation of a previous MQP which initialized the basic design for a tidal turbine. The updated design is comprised of a single neoprene fin that moves sinusoidally in the direction of the flow of water, similar to the motion of an eel's dorsal fin. Both the fin and powertrain designs have been redeveloped for greater power transfer, energy collection efficiency, and manufacturability. Although the power efficiency of the device was not found, the unloaded cut-in speed was measured as 0.7 m/s. It was determined that a lighter, continuous fin is necessary for smoother motion and for reducing the torque needed during its sinusoidal motion. The crankshaft requires manufacturing that is exceptionally difficult on WPI's campus and may also require use of a different material.

1. Introduction

One of the largest problems the world faces is the ever increasing demand for energy. In 2012, the world used 5.598 Tera-Joules of energy, 2.2 times more energy than it used in 1973. Since then, the demand has been rising nearly every year since 1984 (IEA, 1998). At the same time, carbon dioxide emissions have doubled (EPA, 2015), leading scientists to believe global temperatures may rise between 1.1°C and 6.4°C by 2100 (EPA, 2014). Of all energy generation, only 1.1% was generated from geothermal, solar, wind, tidal and other renewable environmental resources (IEA, 1998). From hydroelectric sources, it is estimated that $5.04 * 10^{19}$ Joules could be exploited annually; however only less than 18% of this is currently being harvested (UNDP, 2000).

Hydropower has long been a staple of human power generation. The water wheel was first used between 300 and 100 BCE by Roman engineers to generate power and provide irrigation (Wikander, 1999). The water wheel became a key industrial object by the Early Medieval Ages, with more than 6,000 existing in England by 1100 CE (Friedel, 2007). Major improvements of the water wheel helped spark the Industrial Revolution by allowing for more efficient processes in factories, and the basic concept can still be seen in hydroelectric dams across the world (Thompson, 2009). Although hydropower has been an established mode of power generation for centuries, its full potential has yet to be taken advantage of by current engineering projects. The untapped power that moving water provides is enough to meet more than 7% of the world's power consumption, equal to that from current hydroelectric and nuclear power generation combined (IEA, 1998).

Much of this latent power resides in the ocean in the form of tidal currents and waves. Tidal energy is both powerful and predictable; critical characteristics for large scale power generation. Harvesting this power would allow for a dependable, renewable and clean power source for coastal communities across the world. Unfortunately, current installations are limited to only a few select locations, and few are found outside of developed countries.

When attempting to solve problems that either have a natural source or deal with nature directly, it can be beneficial to turn to natural solutions as inspiration for engineering. One of these strategies, biomimetics, copies or adapts biological systems for human purposes. Because of aquatic life's natural adaptation to living in and working with water currents for movement, fish and other marine animals can serve as inspiration for engineering designs to harvest power from

the ocean. Specifically, rajiform fish, such as rays, mantas and skates, have very large, flat pectoral fins which produce thrust through long vertical oscillations. Mantas typically use this motion to continually cruise through the water, which makes them ideal candidates for bio-mimicry in designing a hydrodynamic generator. This concept was previously explored by a team from MIT, who created an actuated stingray model to develop water based robots capable of movement with minimal energy expenditure.

The goal of this project was to improve on an existing design of a device that generates electrical power from the flow of water. The device was previously a series of fins that were driven by water flowing past, which in turn drives a shaft that supplies rotational energy to a generator that produces electricity. The project was intended to simplify the existing device, as well as to achieve more efficient conversions of power for a given flow rate of water by improving fin design and material selection. The device needs to meet several key benchmarks including:

- Operation in a totally submerged setting
- Operation such that there are no undue negative effects on the local flora and fauna
- Ability for control and measurement from onboard sensors and electronics

Secondary goals included ease of creation and assembly to potentially facilitate future commercialization, as well as uniformity in materials selection and processing to ease technological and production requirements. These goals were of secondary importance due to limitations, such as operational environment, and these limitations may dictate or limit the range of options available to meet the secondary goals.

Testing was accomplished by pulling the mechanism through a standing body of water at a known rate. Performance was gauged based on ability of the fin to turn the driveshaft, turning the rotation into electrical power. The design was originally to be tested with two different shafts to allow for generalizations and correlations to be made which would provide paths for larger iterations in the future. However, only the crankshaft was tested due to unforeseen circumstances with the camshaft.

2. Background

As the world's growing population emits an increasing amount of atmospheric carbon pollutants due to increased energy consumption, the average global temperature rises at an alarming rate. Developed countries have begun to turn to other forms of energy such as wind, solar, geothermal, and hydropower. However, developing countries are still dependent on the usage of fossil fuels. As technology advances, these renewable energy sources have begun to match the world's energy consumption. Hydropower has been evaluated to enhance current technologies to improve power output and efficiencies.

2.1 Current Energy Generation Systems

2.1.1 Energy demand

2.1.1.1 Current Energy Demand in Developed and Developing Countries

Developed countries which are a part of the Organization for Economic Cooperation and Development (OECD), including America, much of Europe, Canada and Australia, currently consume energy linearly with population growth. Developing countries, however, have increasing consumption at a higher rate. In 2014, the world consumed 17.7 Terawatts from all sources of energy (IEA, 2014). Change in energy use was 8% higher in developing countries than in developed countries in 2014 (IEA, 2014). The rate is slowing down for developed countries as goals and standards have been put in place to reduce fossil fuel emissions and focus on renewable energy sources.

2.1.1.2 Forecast

For countries who are still developing, their energy consumption is expected to rapidly increase, accounting for 65% of the world's energy consumption by 2040 (Woody, 2015). It is predicted that as developing countries grow richer and improve their economy, more money will be spent on energy-consuming services. OECD countries are expected to have a slight increase of 0.5% per year which can be accounted for by their population growth while non-OECD countries are predicted to have a 2.2% increase per year as seen in *Figure 1*.

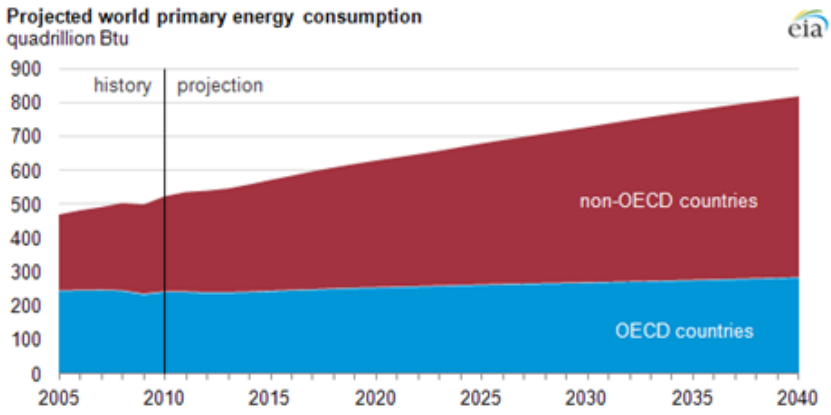

Figure 1: Projected World Primary Energy Consumption (EIA, 2015)

For industrialized nations, regulations have been put in place to help reduce the carbon pollution caused by power plants. For the United States, the Clean Power Plan was enacted in 2015 to reduce carbon dioxide emissions by 32% from 2005 levels by 2030 (EPA, 2015). While developing countries have regulations and laws enacted to decrease the CO_2 emissions, few have been successful in reducing their carbon emissions. Some of policies have been ill-conceived with little resources provided to aid in the development of more effective environmental protection. Once in place, these regulations may lack proper enforcement, causing them to be ineffective in the reduction of fossil fuel emissions and the improvement of renewable energy sources (Issues in Science and Technology, 2015).

2.1.2 Need for Clean Energy

As global energy consumption increases, the greenhouse gas concentration in the atmosphere will also continue to increase. Unless the rate of carbon emissions decreases, temperatures will rise. While the world is already starting to see the effects of global climate change, it is not too late to reduce them. By significantly decreasing the amount of CO_2 emitted into the atmosphere per year, the negative impact of carbon pollution can be stabilized and eventually reversed (EPA, 2015). Many other energy sources produce a minimal amount of CO_2 compared to fossil fuels as seen in *Figure 2* (WNA, 2011). With the use of renewable energy sources, the world can eliminate harmful fossil fuels and instead rely on energy sources that do not have a detrimental impact on the environment.

Technology	Mean	Low	High
	tonnes CO_2e/GWh		
Lignite	**1,054**	790	1,372
Coal	**888**	756	1,310
Oil	**733**	547	935
Natural Gas	**499**	362	891
Solar PV	**85**	13	731
Biomass	**45**	10	101
Nuclear	**29**	2	130
Hydroelectric	**26**	2	237
Wind	**26**	6	124

Figure 2: Energy Sources and their Carbon Footprint (WNA, 2011)

2.1.3 Renewable sources

2.1.3.1 Solar and Wind

The most common renewable energy sources are solar power and wind power as they are readily available and produce very few greenhouse gases. Solar and wind farms are also the most developed technology when compared to other current renewable energy forms. In the US alone, wind energy has enough potential to produce about 10 times the country's power needs (Clean Line Energy, 2015). Both wind energy and solar energy have also become more cost-effective in recent years and are expected to decrease in price in the near future. However, both sources of power require certain climates and geographical areas to be efficient. There must be a sufficient amount of either sunshine or wind for adequate performance of these devices (Prono, 2012).

2.1.3.2 Geothermal

Another solution to reducing the dependence on fossil fuels is tapping into geothermal energy. Available almost everywhere on the planet, geothermal energy works by using hydrothermal convection systems. Cold water seeps into the Earth's crust, heats up, and rises back

to the surface. The hot water is captured as steam and used to drive electric generators. Thus far, 68 billion kilowatt-hours of electricity have been produced (UCS, 2015). With a few power plants however, some air pollutants have been released into the atmosphere. Further research and development is required to improve the geothermal energy harvesting systems.

2.1.3.3 Hydropower

Unlike other renewable energy forms, hydropower is one of the most mature renewable energy sources available currently. It has been used since Ancient Greece and had an increase in popularity during the Industrial Revolution. With current technologies, hydropower has improved greatly to become more efficient and cost-effective. There are now many different forms available including the use of tidal power, reservoirs, and rivers. While hydropower has some disadvantages, overall it is essential to the effort to reduce global carbon emissions (Irena, 2012).

2.2 Hydropower

2.2.1 Turbine power

In 2013, hydropower produced almost 9% of all electricity generated in the United States. Hydropower is broadly defined as power generated from kinetic energy stored in moving water. Typically, this energy is harvested through a turbine, which is embedded in a dam. A properly designed and located dam can generate a megawatt per quarter acre (EPA, 2015), an energy to area ratio more than 20 times better than modern industrial solar installation accomplishments (UCS, 2015). Hydropower also has far lower lifetime emissions than any other industrial sources, producing 46 to 360 times less carbon dioxide equivalent per kilowatt hour compared to a coal-fired power plant (UCS, 2015). These dams are not without drawbacks, however. Dams can have devastating impacts on wildlife, both up and downstream of the dam (UCS, 2015). Upstream, dams inherently flood areas, rendering them uninhabitable for many of its former residents. Downstream, the area may experience greatly changed water flows, especially since dams are designed for constant power generation, as opposed to matching seasonal water flows. This can drastically change the habitats and ecology of land below the dam.

The other major form of hydropower is called hydrokinetic generation. This is characterized by machinery that collects power from moving water without a dam that are typically installed offshore in coastal areas. Current systems include devices that travel vertically with wave motion, pressurizing a gas that is used to produce energy. Another device is a floating reservoir which is filled with breaking waves that drive a turbine (UCS, 2015). Other hydrokinetic systems are powered by currents, using the flow of water to spin a turbine or propeller system. These various forms of hydropower produce different amounts of power as seen in *Figure 3* which allows for a wide range of application depending on the power required (NCI, 2009).

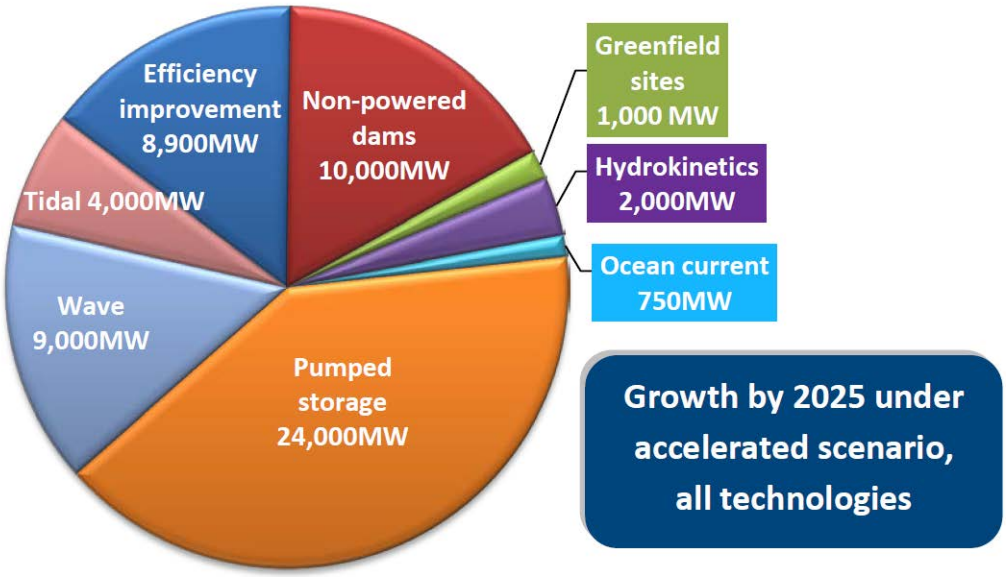

Figure 3: Power Collected from Various Sources (NCI, 2009)

Current kinetic energy generation systems are currently less cost effective than most other forms of power generation. Hydrokinetic generation is roughly twice as expensive per kilowatt hour generated as wind energy (USC, 2015). However, proposals of new projects estimate the costs to be comparable to wind generation, which itself has become 3 to 4 times more cost effective than at its introduction. The levelized cost of energy in dollars per kilowatt hour for varying types of energy generation can be seen in *Figure 4* below (GEG, 2015). Installations are also vulnerable to environmental impacts, such as corrosion or interference from the various lifeforms living in the ocean. The next generation of hydrokinetic generators should therefore be thoroughly designed

to withstand the harsh environment of the ocean while simultaneously being gentle enough to avoid damaging both the generator and the environment around it.

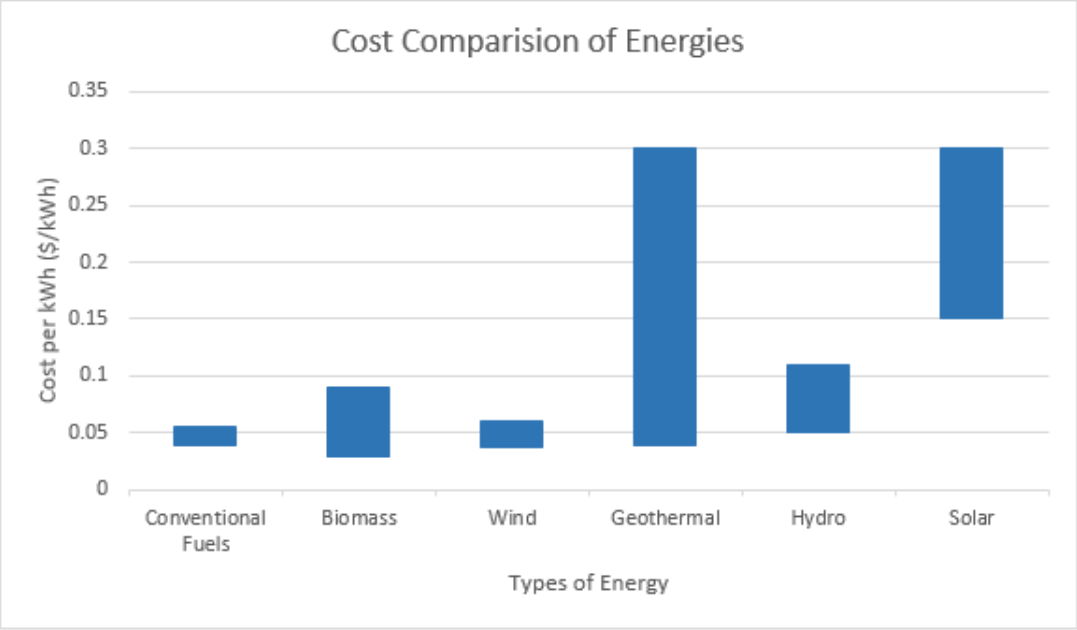

Figure 4: Cost Comparison of Energies

2.2.2 Previous Hydropower Designs

Hydropower has been harvested from sources such as tidal currents and shore waves. The Engineering Business Ltd. (*Figure 5)* has been developing a submerged airfoil-like oscillator. As tidal currents flow over the foil, the device oscillates vertically to pump hydraulic cylinders and drive a hydraulic generator (DTI, 2001). A program logic control (PLC) tracks the system's parameters, including inflow velocity and arm position, to calculate the optimum angle of attack for that instant (DTI, 2003). A major limitation is the energy spent on actuating the hydraulic cylinders to dynamically change the foil's angle of attack (DTI, 2005). The estimated output capacity was 150 kW.

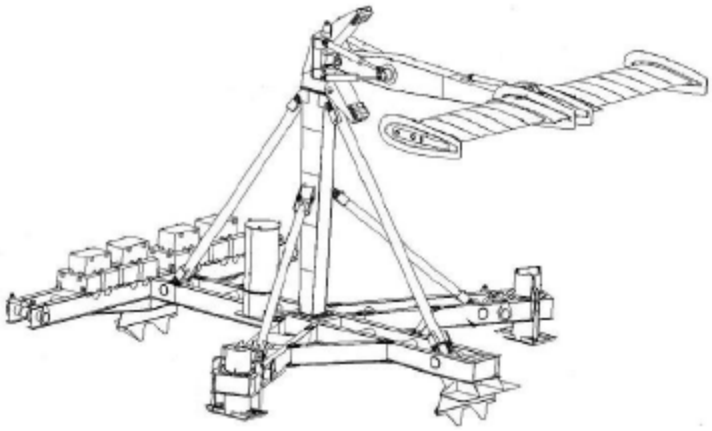

Figure 5: Engineering Business Ltd Model

Under TidGen, a series of cross-flow turbines has been under development. The device captures shallow tidal currents at depths of 15 to 30 meters below the water surface. As current flows against the series of helical turbine blades, the turbine rotates and drives a shaft to the generator as seen in *Figure 6*. The expected peak outputs are 180 kW. One limitation of this design is the lack of yaw, restricting the device to capturing flow along an axis. Because a transmission line will connect directly to the generator, the design must also be robust, being capable of withstanding the pressures at installation depths while being waterproof.

Figure 6: TidGen Model

2.3. Biomimicry and Biological Systems

Biomimicry is the process of copying or adapting something found in nature to address human needs. This has been used successfully in the past to create ubiquitous systems such as Velcro and self-healing materials. This project focused on changing fish locomotion to power production, effectively reversing the natural process

2.3.1 Fluid dynamics of fish

Through years of evolution fish have evolved into thousands of different species. These species have evolved to have a large variety of fin designs for locomotion. Many of these fish have high-performance locomotive properties. It is these properties that make fish ideal subjects of study for both underwater vehicles and underwater energy harvesting devices. One common characteristic of all fish propulsive systems is that they use multiple control surfaces to swim by producing thrust and balancing torques (Lauder and Drucker, 2004). These control surfaces have three main groups: paired fins, median fins, and the body of the fish itself (Blevins and Lauder, 2012). Paired fins commonly consist of pectoral and pelvic fins. There are commonly three types of median fins: the dorsal, anal, and caudal fin (Lauder and Drucker, 2004). A fish can have more or fewer fins depending on the adaptations of the fish and the environment that it is living in. However, for all fish, there exists a body wave that travels along the body of the fish opposite the direction of the fish's movement (Xuelei et al, 2014). This body wave is what allows the fish to propel itself. Although there are many different modes of swimming in fish, this paper will focus on the rajiform and the anguilliform models

2.3.1.1 Rajiform models

Rajiform motion is common in rayfish. This motion uses paired fins for propulsion, as opposed to using whole body motion, and has two common modes (Boileau, 2002). The first mode is oscillatory motion, where the pectoral fins oscillate, propelling the fish. Oscillatory motion is similar to a bird flapping its wings as it flies (Rosenberger, 2001). With less than half of a full wave of the fin, the fish is able to move its fins from its lowest to its highest points. Manta, eagle, and bat rays all use this type of motion. The second mode is undulatory motion, which is defined

by undulation in the pectoral fins where the fins have more than one wave present at a time. Skates and most stingrays use this form of motion for propulsion (Boileau, 2002). Between these two modes, there are large variations in fin-beat frequency, fin amplitude, and the degree of undulation. Undulation motion has a high fin beat frequency and low amplitude. This allows for high maneuverability, quick turning and moving at slow velocities. Oscillatory motion has a lower frequency and a higher amplitude, and generates lift (Boileau, 2002).

2.3.1.2 Anguilliform models

Anguilliform motion is common in long bodied-forms of fish such as eels and lamprey (Vorus and Taravella, 2011). Anguilliform fish use lateral body undulations of their elongated and flexible bodies to swim, using their bodies to propel themselves as opposed to using fins. Anguilliform motion allows the fish to maneuver easily and gives them a unique backwards motion pattern (Boileau, 2002). The undulation amplitudes increase from snout to tail-tip in forward motion (Herral, et al, 2011). The opposite is true for backwards motion. The undulation frequency increases with swimming speed in both forward and reverse motions, with undulation frequency in reverse motions greater than forward motion. The amplitude and wavelength of undulation differ significantly for forward and backwards motion. The undulation frequency is related to swimming speed: however tail tip amplitude, wavelength, and stride length are not (Herral, et al, 2011).

2.3.2 Energy generation

Most previous research on biomimetic fins has been focused on driving the fins through an electric source, whereas this project seeks to accomplish the reverse. As previous research indicates that electricity to mechanical conversion is possible, then the reverse should be possible as well. Of these studies, one reported typical efficiencies of electrical power to locomotive power between 0.08% and 0.153% (Epstein et al, 2006). While these are very low efficiencies, this study was focused entirely on generating motion and largely ignored efficiencies in conversion. Since this project looks to take conversion efficiencies into account, it can be reasonably expected to see much higher efficiencies. This previous research was a robot that was mimetic of a stingray, whereas this project was mimetic of an eel. The previous MQP this is based on achieved 20%

efficiencies in certain circumstances, indicating that this may be a highly promising path to future power generation (Costanzo et. al, 2015). This project intends on improving on the previous MQP, so less internal losses are expected, and thus a higher total efficiency.

2.4. Previous paper

A previous Major Qualifying Project, titled *Design of a Novel Concept for Harnessing Tidal Stream Power*, is the basis of this current project, in which the previous project team designed and manufactured a prototype of the water energy harvester that the current group plans to improve upon. The previous design consisted of a sinusoidal fin made out of neoprene and acrylic with a length of 76.2 cm. The fin drove a camshaft which converted mechanical motion into electrical power via shaft rotation as seen in *Figure 7*.

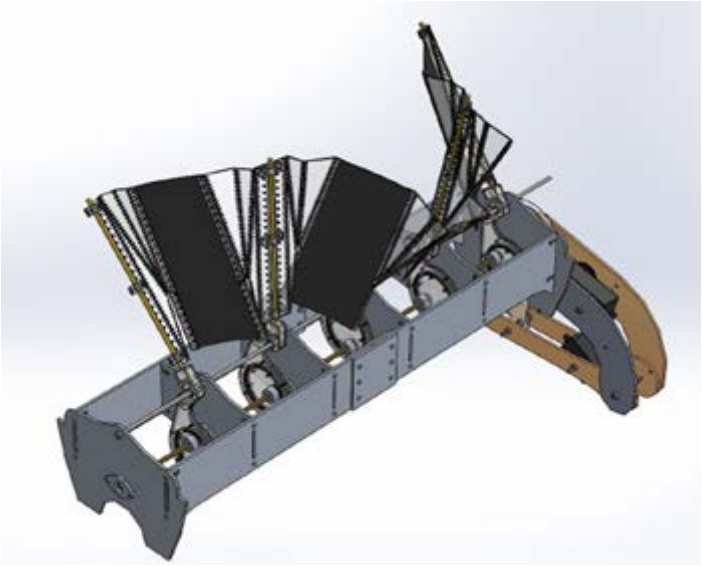

Figure 7: CAD Model of Previous Project

2.4.1 Successful aspects

2.4.1.1 Functioning prototype

The previous project group was successful in building a functional model that effectively produced power in a test setting. Some aspects of their design could have been improved upon, but the prototype did produce repeatable results, with the hybrid acrylic-neoprene fin producing 35 RPM at a flow speed of 1230 mm/s. This translated to roughly 5.5 N*m of torque and 2.8 Watts

of power. Originally, the design called for a full neoprene fin due to its desirable material characteristics; a hybrid fin of neoprene and acrylic was tested, but was far more prone to folding.

2.4.1.2 Mathematical basis

In order to determine the geometry of the fin, the previous group calculated that the flattened form of the sinusoid would produce an arc with a width that was equal to the height of the fin. In every case, the bottom edge of the fin exists at the axis of rotation, so the bottom segment of the fin, when pulled straight, would become the axis of rotation. The geometry is dependent on the change of angle between cams, the length of the fin, and the radius from the center axis of the top and bottom edges of the fin. Constraints included: the size of the frame, the depth of the testing environment, and the phase of the cams.

2.4.2 Limitations

2.4.2.1 Limited testing

Due to testing limitations, there were many constraints placed on not only the design of the model, but also the type of testing available for use. The first major limitation was the absence of a proper water flow tank on university property. Because of this, the previous group tested their model in the rowing tanks in the athletic facility. Significant drawbacks to this were the inability to control and accurately measure the flow rate in the tank, and restrictions in the depth of the tank which was relatively small (about 35.6 cm). This significantly constrained the design and testing of the prototype.

Another testing constraint that arose was the lack of an inexpensive dynamometer that was sensitive enough to measure the small torques produced by the fin. To remedy this, the project group designed and manufactured their own mechanical friction brake dynamometer, which consisted of two Vernier sensors: a rotation sensor to measure shaft speed and a linear force sensor that would measure the force applied tangent to the shaft.

2.4.2.2 Design Flaws

While designing their own prototype, the current project group addressed some design flaws with the original model. The first of these flaws was the design of the hybrid fin. While the

fin was in motion, the acrylic tended to restrict the smoothness of motion of the fin, which would result in a less efficient model than a similar fin made of a single material designed to not lock up. Not only this, but assembling the acrylic and neoprene together was extremely time-consuming, as they were hand sewn together, and increased the possibility of ripping into the neoprene.

The second design flaw rested in the design of the shaft. While the cam shaft theoretically would be efficient at converting the sinusoidal motion into rotational motion of the shaft, there was a significant dwell apparent in the linkage that caused the system to partially lock. This made it difficult to continue to turn the shaft. While it was not as much of a problem for a model of this size, if the project were ever to be scaled up to a working life-sized prototype, this would potentially cause tremendous loss of power and efficiency.

2.5 Summary

Hydropower is becoming increasingly relevant as the need for alternative energy increases. Harvesting tidal energy would significantly increase the amount of energy captured each year through renewable energy harvesting devices. While there are currently many different ways to harvest tidal energy, the search for more efficient methods with fewer environmental impacts continues to be the goal for many researchers and engineers. One novel way to design new tidal energy harvesting devices is through the use of biomimicry, imitation of nature to create designs that suit human need. Through analyzing how fish move through water, this project will focus on designing a new way of harvesting power from water, continuing off of a previous project group's work. This device will mimic the natural motion of fins in order to more efficiently convert tidal waves into electrical power.

3. Methodology

3.1 Improvements

Based on the operation and test results of the old energy harvester, areas of improvement include the fin structure, drivetrain, fin to crank linkage, and torque-reduction gearing.

3.1.1 Fin design

The previous device had two major iterations of fin design. For the first fin, a single neoprene sheet was simply mounted to five radial posts that attached to a rocker arm. The hybrid fin structure featured a series of interconnected acrylic plates and neoprene sheets. The hybrid fin had a similar mounting scheme as the original neoprene sheet, as shown in *Figure 8*. Given the flexibility of the neoprene fin and the lack of support structure, the first fin design was prone to folding under load. However, the flexibility also allowed the mechanism to capture volumetric flow similar to the fins of a fish. In contrast, the composite fin was much less flexible than the first fin. The acrylic plates are limited to hinging about the threaded joints between each other and the neoprene sheets. This restricted movement may explain why the cams had a dwell point, a topic of later discussion. The acrylic plates were also prone to folding in upon themselves, causing the neoprene to awkwardly bend in places.

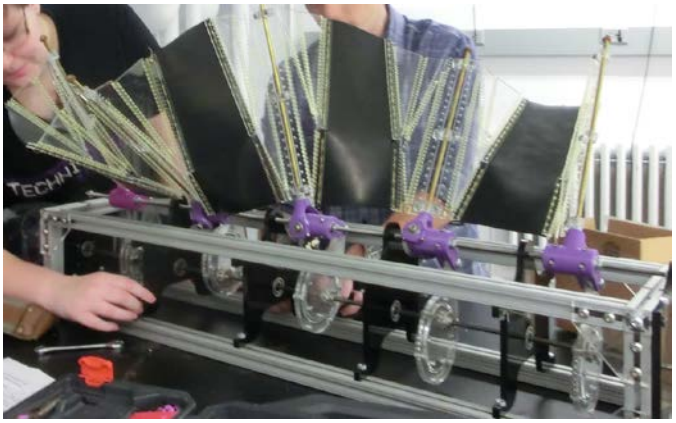

Figure 8: Hybrid Fin Design

When improving the fin design, the device length was kept at 76.2 cm while the number of posts increased from five to seven. Altering the number of posts changed the frequency of the fin and allowed the relationship between the torque-RPM and frequency to be observed by comparing our data to that of the previous team. The transmission angle of 90 degrees was also kept the same in order to compare the effects of changing frequency between designs.

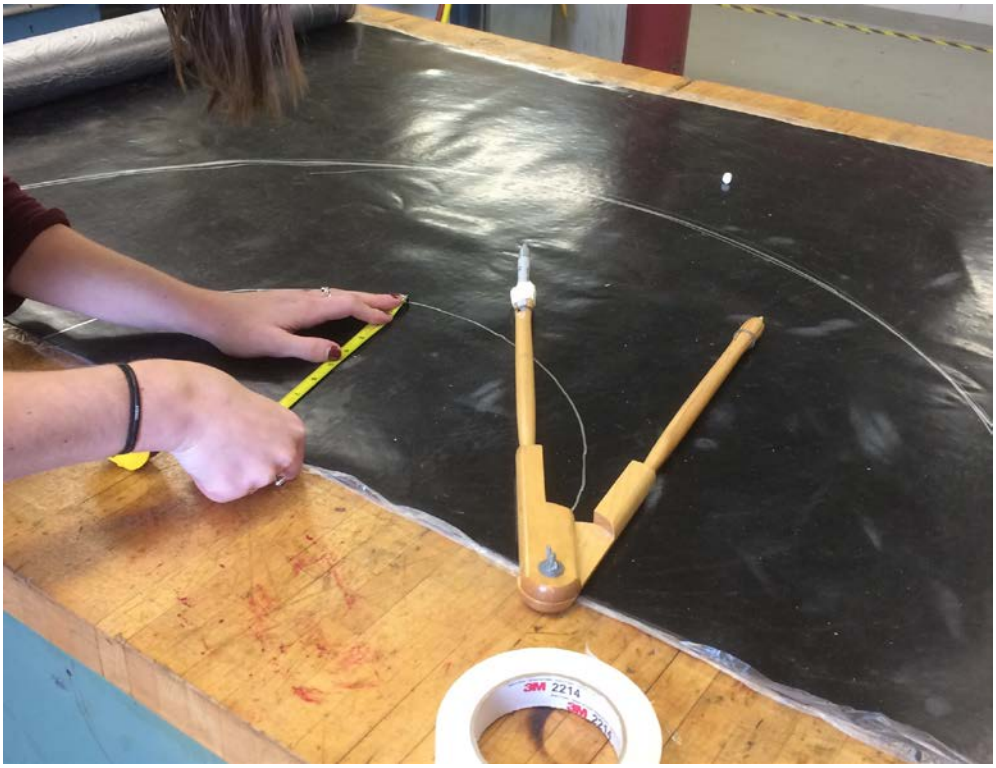

Figure 9: Cutting the Fin

The new design used continuous neoprene sheets much like the first iteration of the previous group's design (*Figure 9*). The new design originally used two sheets of 0.3175 cm neoprene which were glued together with the mounting rods and acrylic supports in between the two sheets. Supports prevented the fin from folding over when held upright. Since assembly was another concern for the fin design, the updated fin simplified the construction as it no longer needed the threaded joints of the hybrid fin. Eliminating the acrylic plating then improved the manufacturability as fewer complex parts and assembly were necessary. The edges of the neoprene sheets were then sewn together in order to prevent peeling of the adhesive used under pressure (*Figure 10*). Manufacturing the device on a larger scale, this could be avoided by using an

industrial strength adhesive. Two sheets of neoprene were later found to be too heavy for the device as it required a large starting torque. The fin was modified to have only one sheet of neoprene with the rods sewn into the fin. This reduced the starting torque required.

Figure 10: Sewn Edges

3.1.2 Drivetrain

Another significant area for design improvement was the use of a camshaft and a crankshaft for the new drivetrains to compare the power delivery efficiency between the two designs. The camshaft followed a linkage design very similar to that of the previous MQP with minor adjustments made to allowing interchangeability with the crankshaft. Based on the same linkage system, the crankshaft design explored the feasibility of its use in a tidal turbine application.

3.1.2.1 Camshaft

To examine how output electrical power to input fluid power changes due to drivetrain design, a redesigned camshaft system and a new crankshaft system were implemented. The

camshaft follows the same basic principle as the old design where a rocker attached to the fin oscillates to push and pull a cam assembly. The cam assembly's motion forces a rotation of an inner disk. Attached to the disk is a driveshaft rotating in place. The new camshaft design reevaluates the linkage system by altering the rocker arm, crank arm, and linkage arm lengths to reduce the possibility of stop points. A significant change between the old and new cam assemblies is the size of the crank disk. With the hybrid design camshaft, there were stick points at certain angles of rotation. Part of this was attributed to the cam design itself, and part of it was due to the fin. Due to extremely tight tolerances in the design and limitations on manufacturing resources, some cams were prone to stick points. These were areas where ball bearings encountered relatively significant amounts of friction that could only be overcome with a certain amount of force. One consequence was that if a single cam lagged, the other cams had difficulty following through with their cycles unless enough force was applied to the system. This created stall points at certain angles of rotation.

3.1.2.2 Crankshaft

The crankshaft is a new design exploring how friction affects the electrical power output to fluid power input efficiency. By reducing the total number of moving parts (i.e. eliminating steel ball bearings), the crankshaft is only affected by friction between the rotating journals and their adjacent webs. Energy from the same rocker system as that of the cam is transferred through a rocker stick connected to evenly spaced journals across the crankshaft. The combined x-y force causes rotation of the journal and subsequently the entire crankshaft. Like the camshaft, the design of the crankshaft was developed using the same rocker-crank linkage path. For easy interchangeability, the crankshaft is spaced such that each journal matched up to the corresponding rocker positioned by the camshaft. The crankshaft output is a shorter driveshaft mounted at the end of the system. The entire system, including the end of the crankshaft, rotates; therefore a continuous driveshaft is not needed.

3.2 Component Design

3.2.1 Fin

3.2.1.1 Fin Shape

The design of the fin was similar to the previous group's design. The overall length of the fin was chosen to be as close to the previous design to make comparisons between the old fin designs and the new fin designs. With a similar length, there was only a small increase in surface area, due to a slightly differing width: therefore the volume of water running over the fin has changed by an inconsequential amount. The number of masts and thus the sinusoidal wavelength created by the fin also increased. The fin was designed to create one and a half periods of a sine wave along its length to increase the frequency of the sinusoid and improve power delivery to the drivetrains. Mathcad was used to determine the dimensions of the design for the final calculations; this can be found in Appendix A. The planar geometry of the fin is an arc section, where the top and bottom edges define the curvature of the wave formed. The fin dimensions include a bottom arc length of 0.77 m and a top arc length of 1.73 m with a radius of 0.30 m between the two arcs. There are seven 0.30 cm masts placed equidistant from each other along the fin.

The geometry of the fin is a function of the angular position of the masts, the total length of the fin, the radius from the center axis to the top of the fin, and the radius from the center axis to the bottom of the fin (Costanzo et. al, 2015). Both the length and radius of the fin were constrained based on the testing environment and chosen to match that of the previous model. As in the previous model, the peak-to-peak amplitude of the fin was chosen to be 90 degrees so that the transmission angles at the joint where the rocker connects to either the cam or the crankshaft linkage will be 45 degrees. This angle is a generally understood maximum for transmission angles. The planar geometry of the fin was calculated using the following equations:

$$\lambda = \frac{2\pi d}{\phi n} \tag{1}$$

$$form(x) = \theta max * sin(2\pi \frac{x}{\lambda}) \tag{2}$$

$$edgeL(r) = \int_0^{len} \sqrt{1 + [\frac{d}{dl}((form(l) * r))]^2 dl} \tag{3}$$

Equation (1) gives the wavelength of the fin (λ), where d is the distance between masts, ϕ is the angular position of the masts, and n is the number of masts in a single wavelength. Equation (2) gives the angular displacement from vertical of the fin along its length (form(x)). θmax represents the maximum angular displacement of the fin from vertical and x is the distance along the fin. Equation (3) represents the arc length along the fin, where len is the total length, in this case 76.2 cm, and r is the radius. Equation (3) was used to determine the length along the top and bottom arc of the fin. The final planar fin geometry can be seen in *Figure 11*. Once the planar model had been calculated, a three-dimensional model was then designed in SolidWorks as seen in *Figures 12 and 13*.

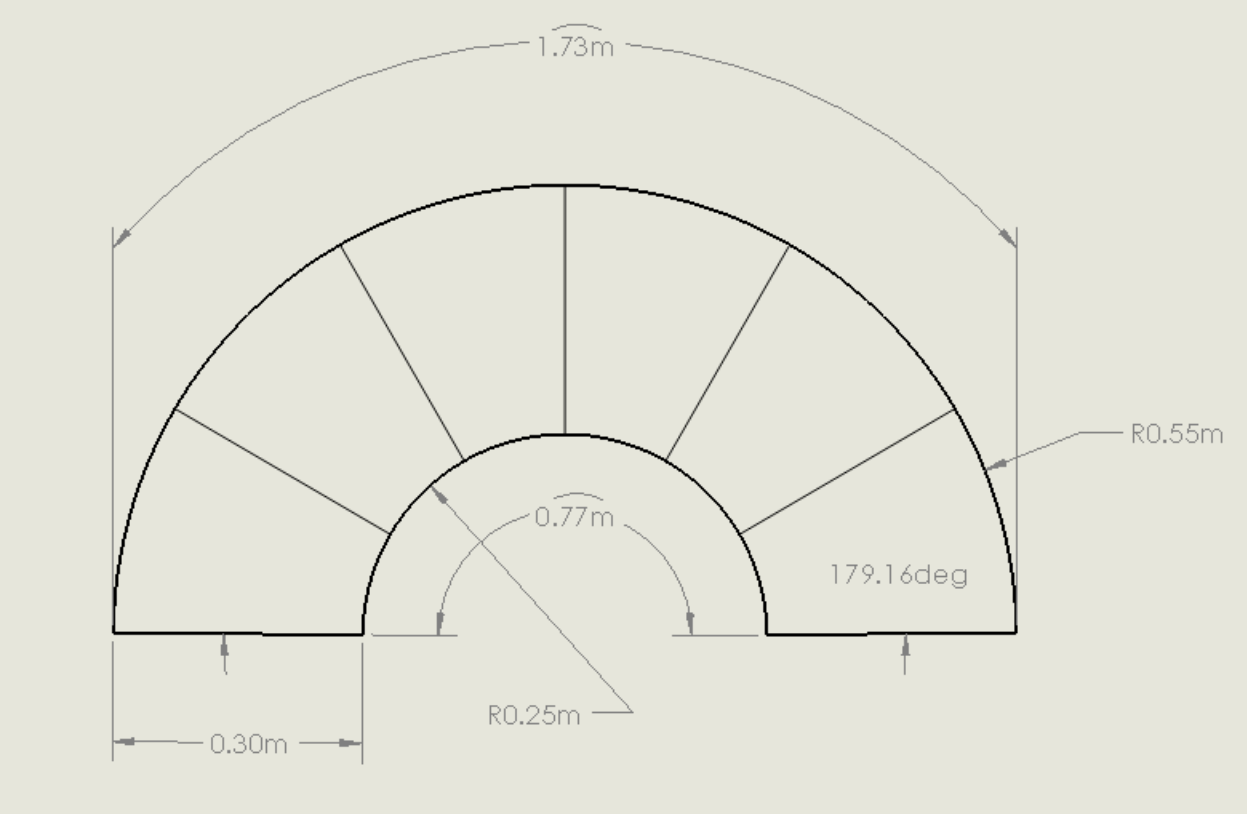

Figure 11: Planar Fin Geometry

.

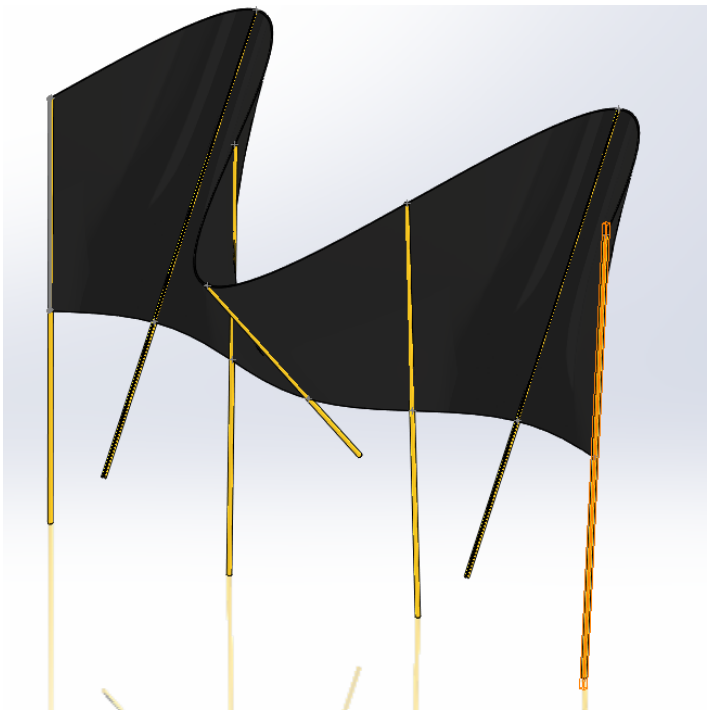

Figure 12: SolidWorks Model of Fin with Masts

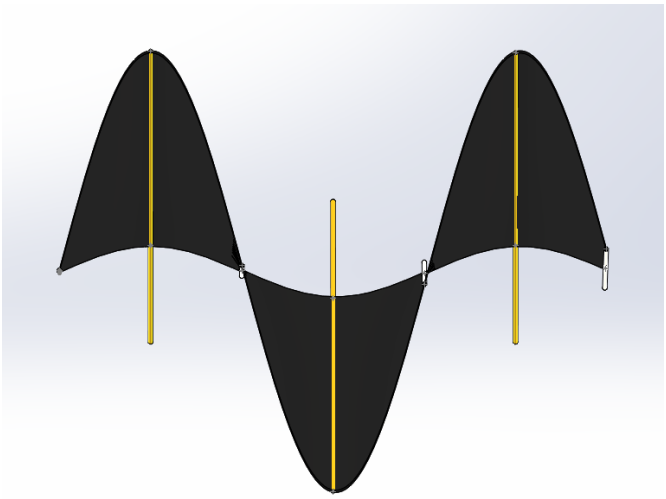

Figure 13: Top View of SolidWorks Model of Fin with Masts

3.2.2.1 Linkage System

The cam and crankshafts were both designed using the same linkage system. This was done to ensure the interchangeability of the drivetrains. The linkage system was designed to be a four-bar crank-rocker linkage using the Linkages Software by Norton. Once the linkage was designed,

it was created in SolidWorks as a skeleton design for the cam and crankshafts. The rocker motion was set at 90 degrees to create 45 degree transmission angles, which is the maximum acceptable transmission angle for a linkage system (Norton, 2012). The linkage system designed is shown in *Figure 14*, the dimensions for this design can be seen in the *Figure 11*. In this design, the rocker drives the crank, which is different from how a crank rocker linkage usually works, where the crank would drive the rocker. In an energy generation system, the masts move with the fin through a flow of water; driving the cam or crankshaft, which in turn rotates the driveshaft which is connected to the motor. The mast connects to linkage system on linkage four. Linkage four is an elbow shape and the mast is press fit into this linkage and held with adhesive.

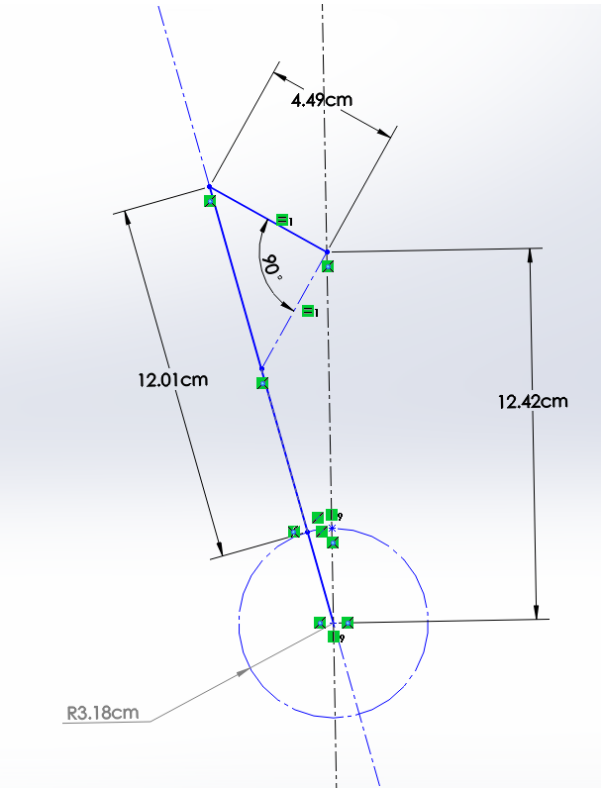

Figure 14: Schematic of Linkage System

3.2.2.2 Camshaft

The camshaft design from the previous MQP suffered from frictional losses and dwell points. The ball bearings frequently got caught on the cam slots, leading to excess friction within the system. Another problem was that the cam would often get stuck when rotating, leading to a

loss of power transmission. There could be several reasons for this, such as a dwell in the cam or a flaw in the dimensioning.

Dynacam Software was used to design the inner cam to produce the 90 degrees needed to create the sine wave in the fin. After the inner cam dimensions had been determined, a SolidWorks model was created for this inner circle. Once the inner cam was designed, it allowed for a design for the outer piece of the cam so that the shape matched the dimensions of the four-bar linkage as seem in *Figure 15*. This new design should have no dwell in the cam motion, and the ball bearings fit together with minimal space between each ball. The dimensions to the cam were changed to allow for the cam and crank shafts to be interchangeable.

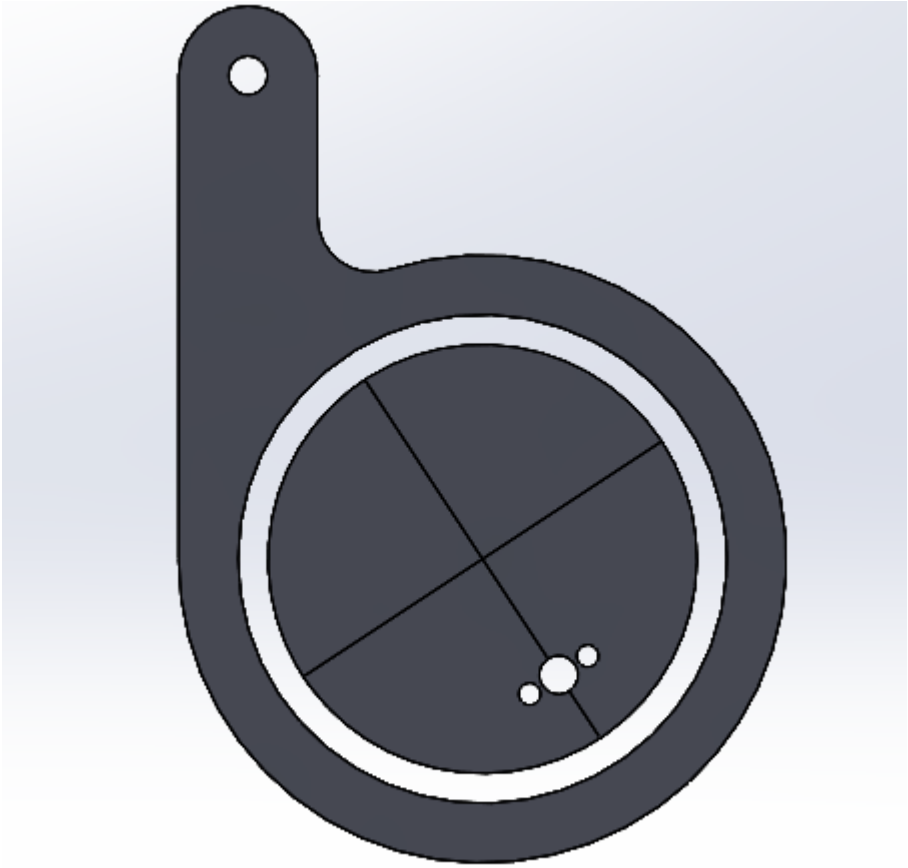

Figure 15: Single Cam in SolidWorks

The eccentric cam converted rotational motion into reciprocating motion. The ribbon fin then transferred rocker motion through a cam that spins an output shaft. The output shaft is a single solid rod that runs through all of the cams. Ball bearings with 0.6 cm diameter were purchased and placed in channels cut into the cams. Ball bearings were used to decrease frictional forces: however there is still friction between the ball bearings and the acrylic with a coefficient of friction of approximately 0.4-0.5μ_s. Graphite lubricant was used to decrease this coefficient. Three layers of 0.32 cm thick acrylic will be bolted together for the outer ring leaving slots for 0.6 cm steel balls to act as the ball bearing assembly. A rocker assembly connects the masts of the fin to the crank as seen in *Figure 16*. The base of the mast is fixed to the rocker linkage. This rocker assembly allows for a 90 degree rocker motion of the masts, that is 45 degrees from vertical each way. The rocker drives the crank causing both the inner ring and the driveshaft to rotate 360 degrees. As the driveshaft rotates, the torque, theoretically, is translated into power using the motor.

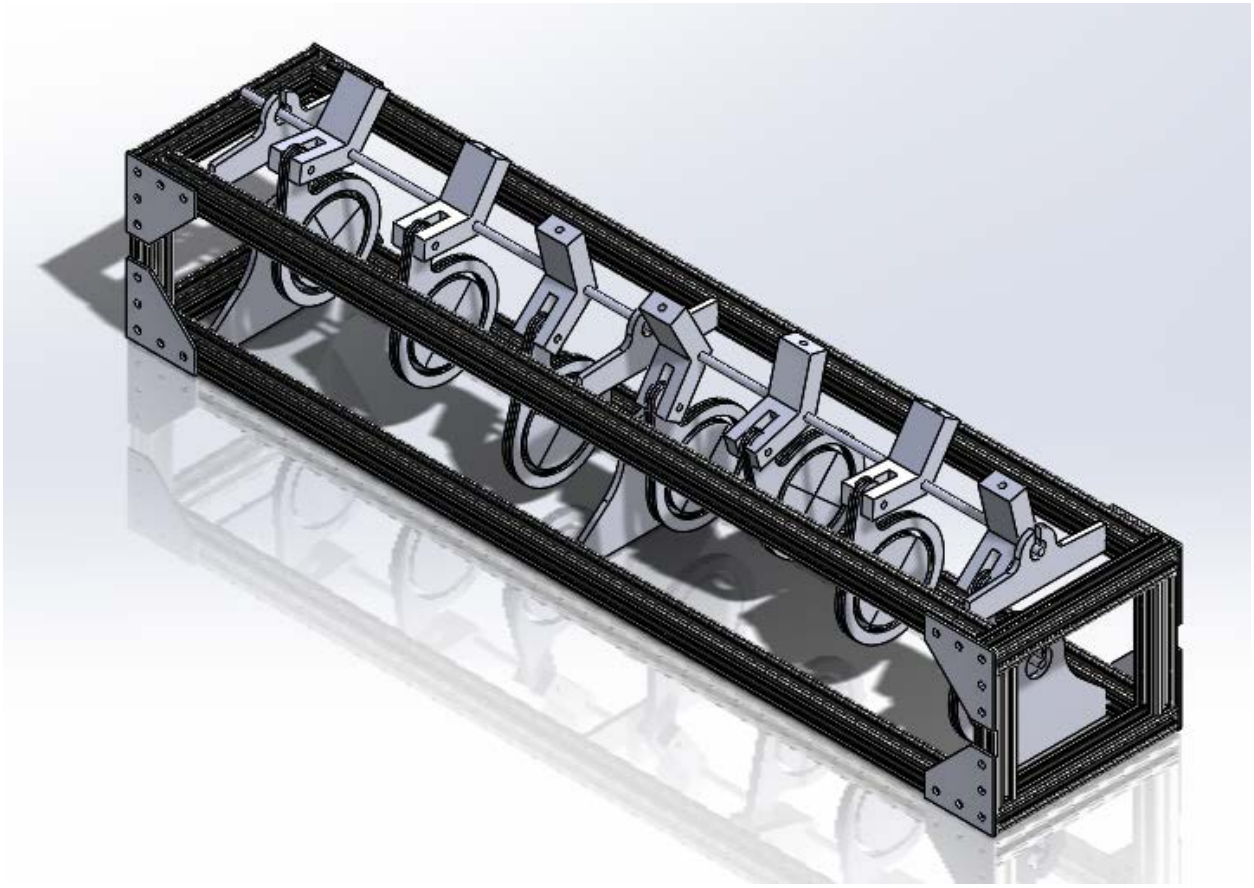

Figure 16: Camshaft Assembly in SolidWorks

3.2.2.3 Crankshaft

Linear reciprocating motion from the fin was converted into rotational motion to a driveshaft via a crankshaft. A crankshaft consists of journals and webs that act as a central drivetrain would. The new design is modular, with separately machined webs, journals, and driveshaft spacers made out of acrylic. The webs and spacer journals are connected using acrylic adhesive and a bolt, preventing the journals from rotating around the flat edge of the webs. On the other side, the true journal was also attached using acrylic adhesive and a bolt, but is cylindrical in shape and has a spinning collar attachment which allowed for connection to the rockers. As force from the rocker linkage was applied to a journal, the journal and web rotated and thus transferred torque to the motor attached in the nacelle. The journal design ensures that all positions of the fin deliver power to the crank regardless of its positioning.

The total effective length of the crankshaft was the same as the total length of the masts, 76.2 cm. The actual shaft length is slightly greater than 76.2 cm to allow for mounting to the frame and attachment to the gearbox. The diameter of the journals was 2.54 cm. Given acrylic's shear strength of 55 MPa, this ensures the driveshaft will be able to withstand the load torque of the water. To prevent interference with the fins and mast, the length between the center shaft and the journal connection was calculated to be 6.4 cm. A hole with depth 0.89 cm was used for the rocker-journal connection. The rocker connects to the journal with a pin that runs through the face of the journal and its connecting webs at said depth. *Figure 17* below depicts the crankshaft mounted to the 80/20 frame.

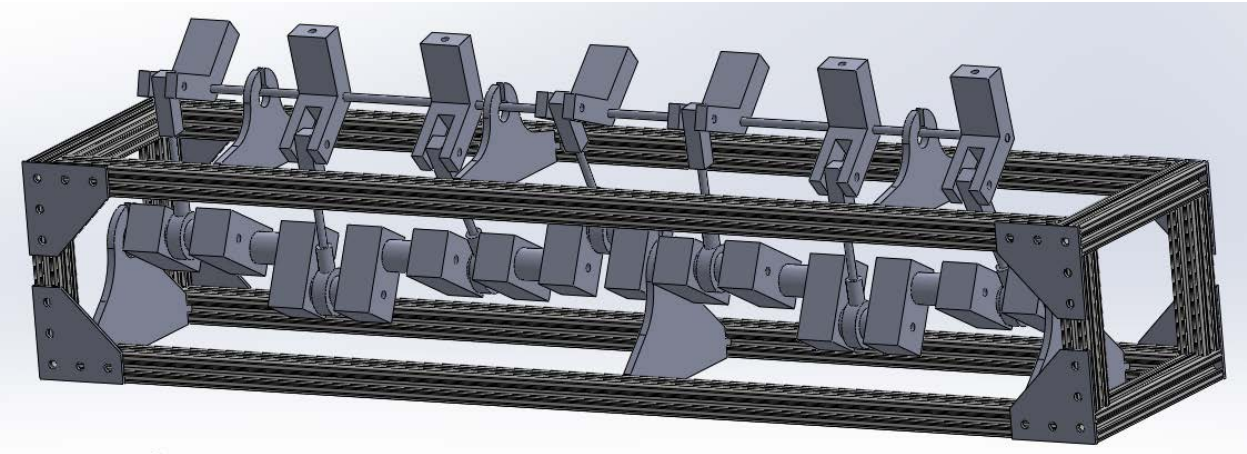

Figure 17: SolidWorks Diagram of the Crankshaft

The crankshaft was mounted in a similar fashion as the camshaft. Bearings supported the ends and central parts of the crankshaft, enabling free rotation in relation to the frame. A gear was attached to the end of the driveshaft to transfer shaft power into the gearbox.

3.2.2 Frame

The 20.32 cm x 17.78 cm x 81.28 cm frame was composed of twelve connected pieces of 80/20 aluminum bars connected with acrylic corner plates. This frame was salvaged from the previous MQP to save time building the overall mechanism and because 80/20 could be easily modified to add external supports. To hold the camshaft and crankshaft drivetrains in the frames, several acrylic support plates are placed across the frame. Both the rocker shaft and the driveshaft have individual acrylic supports to help distribute the weight. These supports use two glued pieces of 0.3175 cm acrylic to reduce the likelihood of deflection. Embedded into the glued acrylic is a single 1.91 cm inner diameter bearing that allows the shafts to spin freely in the support. At the ends of each support plate, there are keys that allow the plates to slide into the 80/20 bars. To ensure the cam and crank follow the correct linkage paths, the support plate bearing holes are offset to be slightly above the upper limit of the frame.

3.3 Material Selection

3.3.1 Materials and Cost Analysis

When selecting the proper materials for construction, cost was a major consideration. However, a balance was struck between material properties necessary for proper functionality and the cost of material. Various components of the design required different materials because they each have different tasks. The camshaft, the crankshaft, the fin, and the driveshaft were the main consideration for this section. For the camshaft, laser-cut acrylic was chosen as it would provide a durable material at a low cost. A 61 x 122 x 0.32 cm sheet of strengthened, UV-resistant acrylic sheet costs approximately $40. This acrylic has excellent tensile strength of 55.16-77.57 MPa at a temperature range of 0 to 78 degrees C. These properties all fall within necessary tolerances based on expected forces. For the crankshaft, acrylic rectangular rods were chosen, despite being more expensive, as it would be easier to drill the holes into the square pieces versus another shape or

material. The cost, however, was only $56.98 for a rod with dimensions of 2.54 cm by 3.175 cm by 152.4 cm and provided the sufficient strength required. The journals connecting the webs for the crankshaft did not need to be drilled vertically and could therefore be cylindrical. For a 61 cm rod with a diameter of 1.27 cm, it would be cost $11.28.

The driveshaft, a steel, hexagonal shaft, was recycled from the previous MQP and was durable, machinable, and mostly resistant to corrosion. This shaft held up to the forces that exist while it converted the rocking motion to a rotating motion. The fin was constructed of fabric-reinforced neoprene as it needed to be flexible yet durable as it moved with the water. This type of neoprene has a tensile strength of 10.34 MPa within an operating temperature range of -34.44 to 93.33 degrees Celsius. For a sheet dimensioned 0.16 by 30.5 by 122 cm, it cost about $75 (McMaster, 2015).

3.3.2 Finite Element Analysis of Components

In order to determine the materials used to create the crankshaft and the fin, CAD models were subjected to finite element analysis (FEA) using Ansys Multiphysics software. Ansys is a powerful physics simulation program that allows direct analysis of CAD files with a number of different modules. Critical for this project, Ansys contains both fluid dynamics and structural analysis modules which can feed results into each other. Using the fluid dynamics module, the forces on the fin model were found and then input into the structural analysis module. The water was defined as flowing at 2.0 m/s, the maximum flow velocity we can expect to achieve in our testing. This was coupled with varying the material composition of the masts. This system is depicted below in *Figure 18*. Materials considered such as brass, certain stainless steels, aluminum and several polymers were required to be corrosive resistant in chlorinated water.

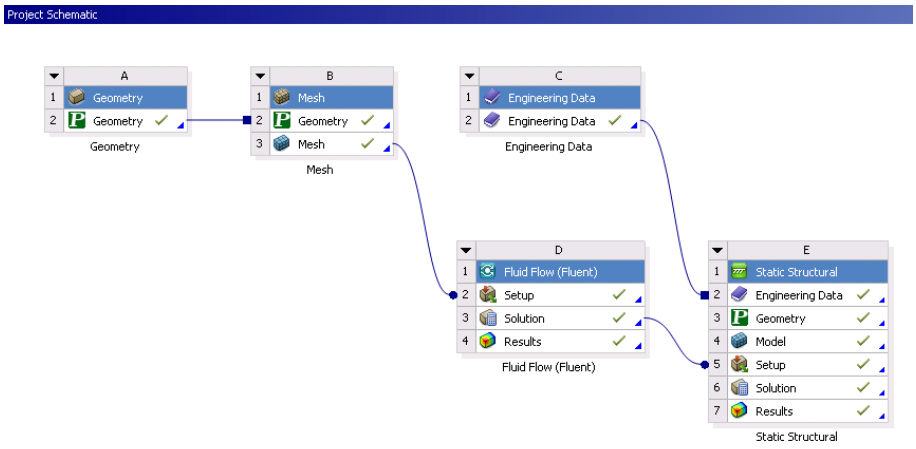

Figure 18: Ansys Simulation Setup

Ultimately, this analysis led to the decision to choose stainless steel to create the rod. It was chosen because it will not plastically deform or suffer brittle failure at the expected loads, while also being the cheapest to procure and the most stable in chlorinated water. A table of the materials, cost and whether it passed or failed the test is below. For the tests, a model of the fin was created and imported into Ansys. Using a computational fluid dynamic modeler, the forces that the mast experience were modeled. This information was then used in a structural analysis of the fin, which was used to determine which materials would withstand the projected forces, shown in *Table 1*. More detailed results of the FEA programs can be found in Appendix 2.

Table 1: Mast Material Analysis

Material	Cost per 30.5 cm length (25.4 cm diameter)	Pass/Fail?
304 Stainless Steel	$2.42	Pass
464 Naval Brass	$6.19	Pass
6/6 Nylon	$0.45	Fail
6061 T6 Aluminum	$2.00	Pass
Polycarbonate	$1.22	Fail

The crankshaft was also designed using FEA. The major consideration in designing the crankshaft was the material selected. The initial crankshaft design called for the use of 6061 aluminum components. However, aluminum is both more expensive at $\$0.0418/cm^3$ compared to $\$0.0277/cm^3$ for acrylic. Aluminum also requires more tooling and longer cycle times than acrylic. Therefore, FEA was used to determine if acrylic was strong enough to withstand the forces that would be experienced during operation of the device. A load of 6 N was applied on each crank journal, well in excess of the equivalent force to create the 3 N*m total torque measured in the previous experiments, and placed bearings each support journal. The loading can be seen in *Figure 19*. These calculations demonstrated that the stresses experience would remain within the plastic deformation range. The tensile strength of acrylic is 69 MPa at yield, and the compressive strength is 124 MPa yield, both far surpassing the calculated stresses on the crankshaft. Acrylic has a shear strength of about 62 MPa, which is more than two thousand times the shear stress experienced by the shaft, as demonstrated in *Figure 20* and *Figure 21*. While the model assumes that the loads will be applied directly in line with the journals, this is unlikely to occur in testing. However, the acrylic so vastly outperformed the tests, it is reasonable to believe that it should be able to survive any misaligned loading.

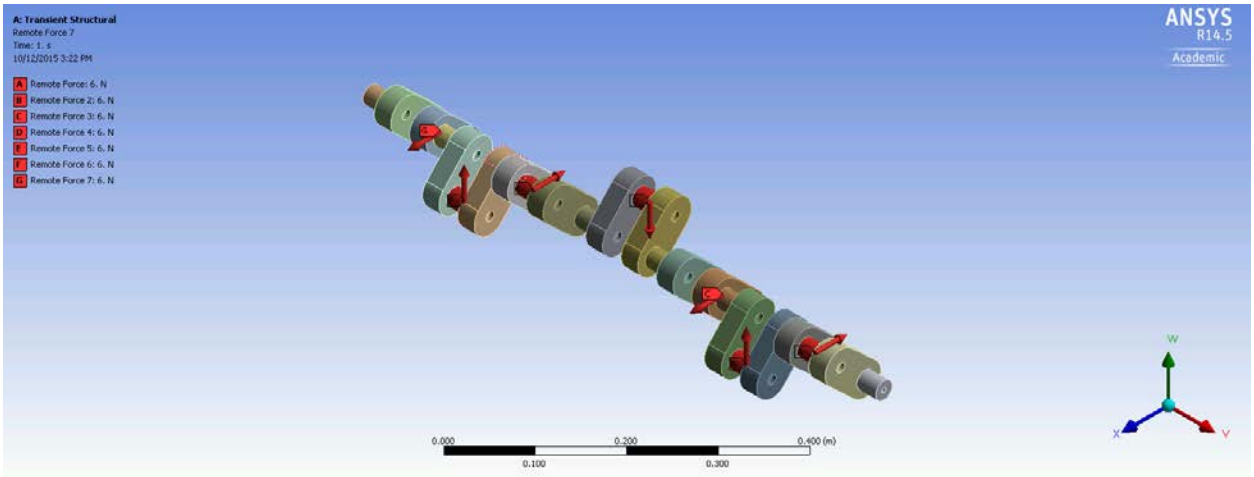

Figure 19: Crankshaft Loading

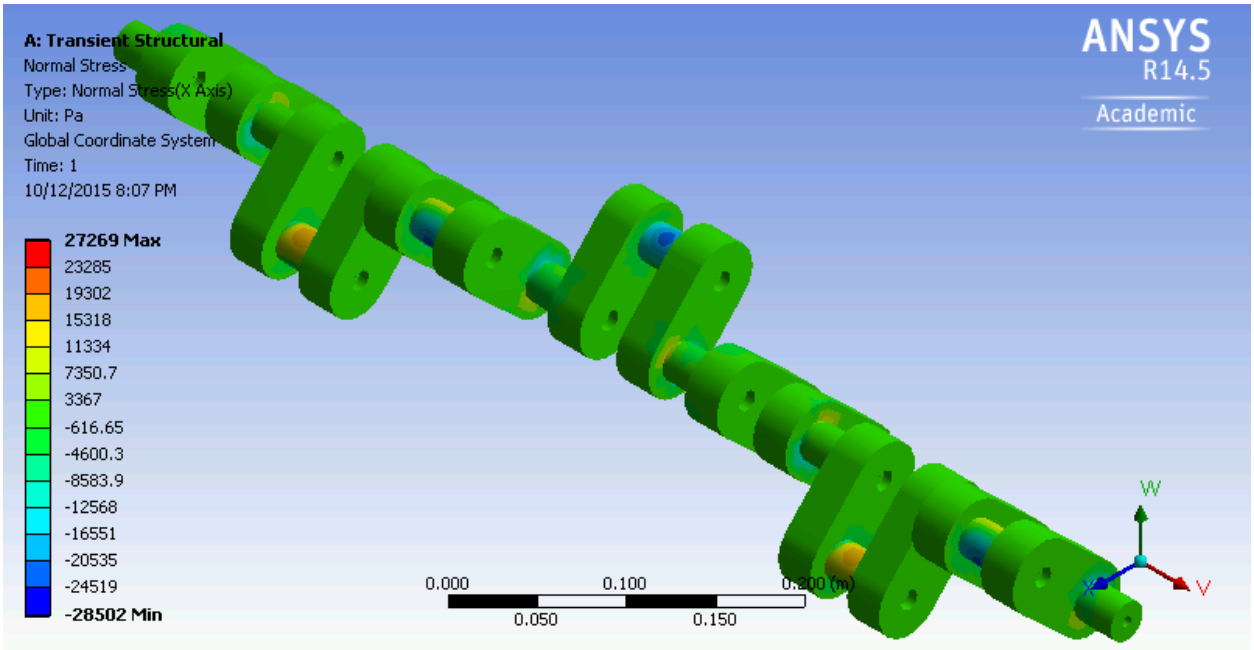

Figure 20: Normal Stress Calculated by Ansys

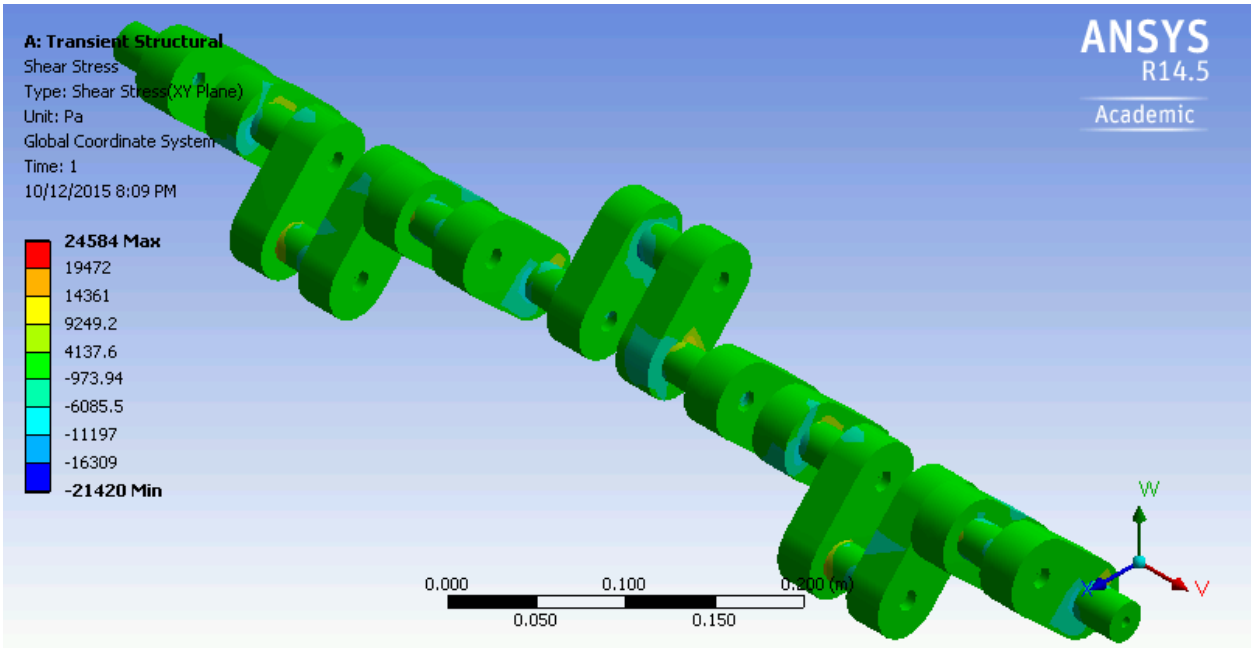

Figure 21: Shear Stress Calculated by Ansys

3.4 Manufacturing

All components were designed to be manufactured using local capabilities, such as a CNC mill and a two-dimensional laser cutter in Washburn Shops. These resources allow us to machine a wide variety of part sizes and materials with high tolerances and relatively short cycle times.

3.4.1 Materials

The materials that the design used include acrylic, which was predominantly used in the camshaft and crankshaft assemblies, neoprene sheets, extruded 80-20 aluminum, and brass rods. There were also several driveshafts, bearings, fasteners and supports used, many of which were off-the-shelf products to reduce manufacturing demands. Materials were generally chosen with attention to machinability and stability in water to avoid corrosion.

The camshaft assembly was built with acrylic cams resting on stainless steel ball bearings and mounted on a steel driveshaft. The crankshaft was built from acrylic components bonded with glue and bolted together. Due to the weight of the crankshaft, the shaft was supported by several bearings mounted to 3D printed supports. The fin was built out of brass rods with a neoprene sheet to catch the flow of water.

3.4.2 Production

Generic parts including the bearings, driveshafts, and fasteners were obtained off-the-shelf. The custom created parts were machined using a variety of tools, including vertical CNC mills, a laser cutter, and a MakerBot 3D printer.

3.4.2.1 Rocker Production

Rockers were designed and printed to mount directly to the fin masts. All seven rockers were printed out of ABS plastic using a 3D printer. The rockers were then mounted onto a ¼ steel shaft and locked in place by securing a threaded nut with Loctite on each side of all of them. The camshaft attaches directly to the rockers with bolts. The crankshaft is attached by aluminum rods that are mounted to 3D printed ABS blocks, which are bolted into the rockers using the same scheme and hardware as the crankshaft.

3.4.2.2 Camshaft Production

The camshaft was machined using a VLS 4.60 Laser Cutter. This allowed parts to be directly converted from SolidWorks drawings to machine instructions, facilitating easy production of many identical components. Due to the size limitations of the laser cutter, acrylic pieces needed to be created in multiple parts and bonded together. Typical acrylic glue was used to weld the pieces together, achieving a bond strength around 14 MPa, far exceeding the calculated loads.

During machining tolerances and the need for high tolerance pieces, several iterations of the camshaft were cut and tested until a design was achieved that both securely held the ball bearings in place and allowed for the free rotation of the cams. A total of 33 iterations were tested: between each iteration the inner and outer circles of the cam design were changed by hundredths of an inch. Notably, the middle cam had a slightly large cut to create a channel in which the ball bearings could rest.

Once all the acrylic was cut, the cams were assembled. Each cam contained six ⅛ inch thick acrylic pieces, ¼ inch diameter ball bearings filling in the space between inner and outer pieces. The six acrylic pieces can be seen in an exploded view in *Figure 22* below. The cams were assembled by first aligning and bonding together one of the out cam pieces with the center piece, making sure that the holes for the shaft were aligned. Next, the balls were placed into the ring made by the inner circles and outer cam piece. Lastly, the second outer piece was aligned and bonded. The cams were then held in place with a clamp to allow to bonding agent to properly bond the pieces together. This method was chosen over notching the acrylic to fit the bearings in because it was less likely to damage the acrylic and it was less likely the bearings would pop out when pressure was applied.

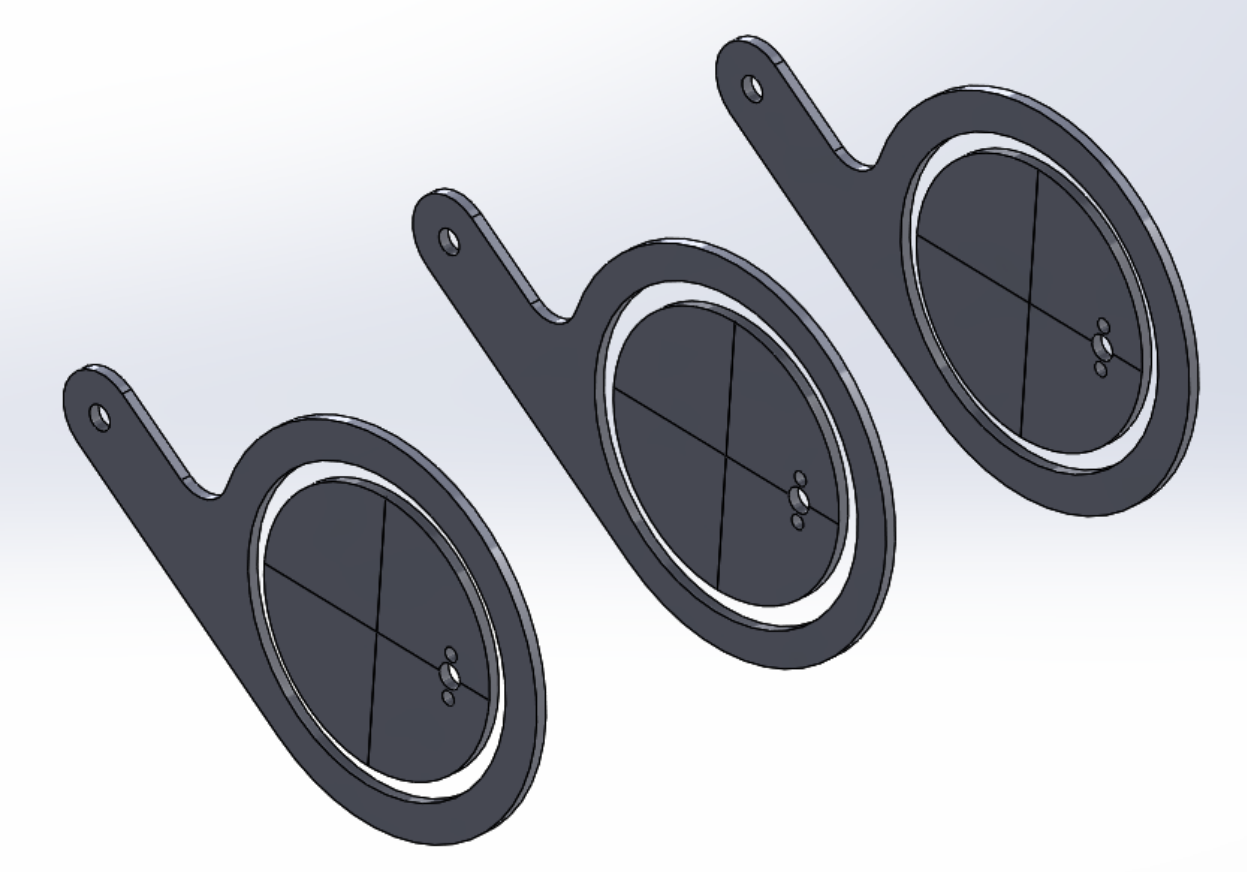

Figure 22: Exploded View of One Cam Assembly

3.4.2.3 Crankshaft Production

The acrylic components of the crankshaft were machined using a bandsaw, while CNC mills were used to drill all necessary holes. The crankshaft was machined and attached in pieces to ease manufacturing and lower costs. The shaft was created using an acrylic rectangular rod and a round rod. The pieces were cut to length using the bandsaw then both bolted and bonded together to ensure the journals and webs would stay at the proper angle relative to each other as seen in *Figure 23*. The round rod was used for the webs and was connected to the rockers using bearings with 3D printed sleeves that hold an aluminum rod. Another 3D printed piece was printed to hold the other end other the aluminum rod to the rocker. A stainless steel driveshaft was purchased to avoid a high tolerance machining operation, as well as the providing the benefit of being completely stainless with no risk of damaging the finish during manufacturing. The drive shaft

was connected at the end of the crankshaft and is connected to the motor through a Lovejoy coupling.

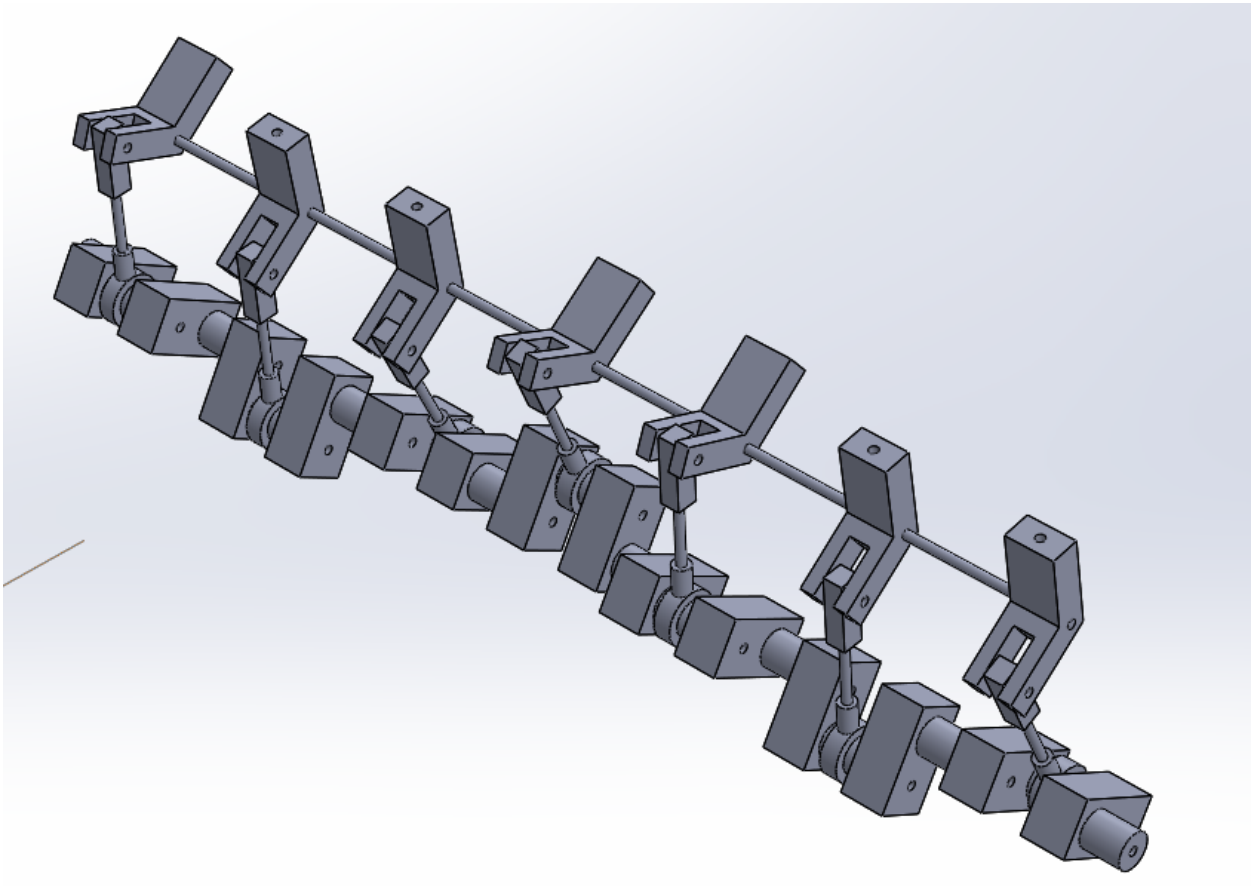

Figure 23: SolidWorks of Crankshaft Assembly

3.4.2.4 Frame Production

The test frame is made of 80-20 aluminum. The shafts are supported by off-the-shelf bearings mounted in sheets of laser cut acrylic. This was necessary due to the weight of the crankshaft and the deflection of the rocker shaft. The camshaft and crankshaft use an interchangeable mounting scheme so that they can quickly and easily be switched to facilitate testing. The fins were originally permanently mounted to rockers, which had interchangeable mounting scheme so that they could easily be mounted to either the camshaft or the crankshaft. It was important to minimize changes between the different device configurations, to allow accurate direct comparisons of device performance between the cam and crank shafts.

3.4.2.5 Fin Production

The first fin iteration was originally constructed from two sheets of 0.3175 cm thick neoprene manually cut into the shape as seen above in *Figure 11*. The two halves of the fin were glued together using 3M Hi-Strength 90 spray adhesive. Supporting masts were placed between the two sheets at predetermined intervals prior to gluing the two halves. The bottom of each mast was approximately 5 cm from the rocker edge of the fin. To mount the fin, the adhesive glue was applied to each of the masts which were then inserted into the rocker mounting bore. Due to issues with the crankshaft movement caused by the overall weight of the fin and the shape of the fin, a second iteration of the fin design was pursued. The new fin was constructed from a single sheet of neoprene supported by embedded masts. 2.5 cm of fin material was removed from the bottom edge of the fin. This was done to account for the fact that the original fin was meant to be placed only 2.54 cm from the point of its rotation but with the rockers in place the fin was approximately 5 cm from that point. Masts were sewed into the neoprene using thread. The locations of the embed points were manually adjusted such that the fin better followed the intended sinusoidal motion. Masts were placed 2.5 cm from the rocker edge of the fin such that there was no gap when the fin was mounted onto the rockers. Vertical slits were cut down the middle of the fin segments to also match the sine wave. Each slit depth was empirically determined by spinning the crankshaft and locating “catch points.” Slits were then sewed loosely together using jewelry thread for fin continuity. The same fin mounting method was used.

3.5 Testing

3.5.1 Testing Environment

To evaluate both designs using the crankshaft and the camshaft, adequate testing space was needed. The swimming pool located at WPI’s Sports and Recreation Center provided sufficient space to test the designs. By using the school’s equipment and facilities, special consideration was required to ensure damage will be prevented. For this, testing rigs have been designed and constructed for use in the space. The previous testing rig design was used and reconstructed as no problems had occurred when in operation. The rig consisted of a metal frame supported by a set of pontoons allowing the neoprene fin to be the only element of the design exposed to the water.

Because the fin only occupies a fraction of the pool volume, it is assumed to be an infinite body of water. The mechanism attached to the rig was then pulled through the water using rope to simulate a flow on the fin. This design considered the weight of the assembly, portability from one location to another, and ease of assembly.

Once it was determined that no valid data was being retrieved from the pool testing, bench top testing was used. The device was relocated to WPI's ME department MQP lab where bench testing took place. As the device was no longer in water, it was inverted and the pontoon rig was removed to be placed on a bench for further testing.

3.5.2 Testing Procedure

The original testing procedure was written to be used on both the camshaft and crankshaft. However, complications occurred with the mechanism which did not allow for testing for data involving the power output. In the following procedure, the electrical system collects rotational speed and electrical power output data. This procedure is as follows:

- Set up device with crankshaft as the driveshaft
- Attach the nacelle to the device
- Place the testing rig into the water
- Place device into the testing rig
- Hook the rig up to the guide ropes and winch
- Pull the device across the pool at different speed intervals of 0.5 m/s with an initial speed of 0.5 m/s
- Repeat the process to a maximum speed of 3.0 m/s
- Repeat the procedure with the camshaft
- Remove device from pool
- Detach the guide ropes and winch from testing rig
- Remove testing rig from the water
- Compile data into Excel file

After initial testing in the pool, it was determined that the device would not provide the data needed for accurate results as it only would spin for two cycles before the acrylic bonds broke,

halting movement of the shaft. Several new procedures were therefore developed for bench top testing for only the crankshaft. Due to limited time, several new procedures were therefore developed for bench top testing of the crankshaft only. The following procedure determined the maximum amount of weight the driveshaft could sustain.

- Add weights to the outermost ends of the masts
- Turn the wheel attached to the crankshaft to see if the driveshaft would complete a rotation
- Increase the amount of weight by 50 gram increments per mast
- Repeat this process until either the rocker shaft deflected more than 1 cm or the driveshaft stopped spinning
- Compile data into Excel file

Another procedure was written in order to determine the minimum amount of torque needed to move the fin in the water and is as follows:

- Connect a wrench to the end of the driveshaft so it is horizontal to the ground
- Mount weights to the end of this moment arm and suspend them from free fall
- Release the weights and allow them to drop and pull the wrench
- Increase the amount of weight by 50 gram increments
- Repeat this process until the crankshaft rotates
- Compile data into Excel file

3.5.3 Testing Variables

For the performance of the device to be properly evaluated, several variables of the device and testing environment were to be manipulated. However, in order to facilitate the comparison of this design with the previous design many of the testing variables were kept the same as they were for the previous design. Therefore the independent variables and dependent variables were fin configuration, fin height, flow velocity, torque, shaft type, rotations per minute (RPM), and power output.

For this experiment both the fin configuration and fin height were kept the same throughout testing. This constant was chosen in order to compare the design of this project with the fin design of the previous MQP. This choice was also made due to time constraints as it was

infeasible to test both a cam and a crank shaft designs for more than one fin model in the time period given.

The flow velocity was determined to be an independent variable. By varying the flow velocity the device can be tested under different flow conditions and an ideal flow velocity could be determined based on a power curve created over the range of flow velocities. In order to test for flow velocity, a motorized winch was used to accurately pull the rig at a constant speed that was changed after each test.

The shaft type was varied between a cam shaft and a crankshaft. The shafts were interchangeable and half the tests were performed using the cam shaft, while the other half of the tests were performed using the crankshaft. These two designs were interchanged in order to test the theory that a crankshaft is better suited for this device. The power outputs and efficiencies of both shafts over the range of flow velocities were plotted and compared in order to determine which shaft is a better design choice. The torque was varied using a mechanical device. The torque was varied to represent different loads that could be attached to the shaft in order to determine the range of the device.

One dependent variable of these tests was to be the output from the motor. The power output is most indicative of the performance of this device and was to be measured using the data produced by an electric motor.

Once it was determined that the pool testing no longer viable, new testing variables were chosen. Both bench tests were used to calculate the torque along the shaft. In both tests the independent variable was chosen to be the weight added to the system. The moment arm was kept as a constant. Therefore the torque on the system became the dependent variable.

4. Results

4.1 Pool testing

Initial testing in the pool (*Figure 24)* was unsuccessful due to a number of reasons. Primarily, the bonding agent holding the crankshaft together was not holding and the shaft would begin to rotate freely about itself. The harvester had relatively heavy components as well as several sticking points in its free rotation. This meant that a large amount of torque was required to begin spinning. The amount of torque required led to problems with the crankshaft due to its construction. The shaft was built out of acrylic blocks that were both glued and bolted together. The torque required to spin the fin were also large enough to break the glued surfaces apart. This was a massive problem, since the harvester was damaged by itself during operation. The best way to address this would be to use different glue or attachment mechanisms or simply use a solid, single piece design for a driveshaft.

Figure 24: Testing Rig in the Pool

Another problem experienced was the difficulty in achieving a straight line of travel through the pool. Without a mechanical or automated winch, it was exceptionally difficult to keep a constant speed as it was pulled through the pool. Guide ropes were used to keep the device traveling in a straight line along with someone swimming along with the device correcting any directional changes as necessary.

Although no power efficiencies were able to be tested for, an unloaded cut in speed was able to be determined. The device was pulled through the water at 0.5 m/s and the drive shaft did not spin. The device was then pulled at 1 m/s and the drive shaft spun with no visible difficulty. It was therefore determined that the cut in speed is estimated to be around 0.75 m/s. Using this estimated cut in speed the approximate torque of the water can be calculated to be 1.228 N*m as seen in Appendix C. Using video of the pool tests it was determined that the fin moves approximately 90 degrees in 2 seconds when pulled through the water at 1 m/s, this translates to the crankshaft moving at approximately 7.5 RPM. This angular velocity is comparative to the previous year's design which was running at a range of 6-35 RPM for their hybrid fin, which had the best performances of last year's designs. Using these results the ratio of $\omega R/U$ is 0.25. Where ω is in rad/sec, R is the length of the fin in meters and U is the flow speed of the water in m/s.

4.2 Bench Top Testing

Once it was determined that pool testing was not producing any viable data due to the problems with the crankshaft, benchtop testing was used to provide further insight into the torques on the system. This allowed for the calculation of the water velocity needed to drive the system.

4.2.1 Theoretical Ideal Torques

The torques needed to put the fin in motion were calculated based on the weight and shape of the fin and tested by spinning the shaft. The calculations based on the geometry and weight of the fin can be seen in Appendix C. For these calculations it was determined that the center of gravity of each section of the fin was approximately vertically halfway up the fin. With the weight of the neoprene measured at 958 grams and the length of the fin to be 33.02 cm, the torque needed to move the fin was calculated to be 0.259 N*m. This number represents the ideal torque, not taking into account any losses due to friction or other design factors.

4.2.2 Minimum Torque to Spin Driveshaft

The bench top testing of the torques were measured using a moment arm with a known length. Weights were then added at the end of the moment arm as seen in *Figure 25* below. The weight was increased at intervals of 50 grams until a weight of 600 grams was reached. At 600 grams the small weights were exchanged for a 1.5lb (680g) weight as this was the next largest weight available. Weight was then increased by 50 gram increments once again. At 980 grams the weight was able to completely move the shaft without getting stuck at any point. Using the 980 gram weight and moment arm of 110 mm the torque to start the shaft in motion was determined to be 1.057 N*m. The difference in the theoretical and tested starting torques is due to losses such as friction in the shaft. Using this torque, the minimum velocity of water flow needed to spin the shaft was calculated to be 0.696 m/s. This speed matches up with the cut in speed found during pool testing and verifies the results.

$$L_{arm} := 110mm$$

$$W_{fin} = .98kg$$

$$g = 9.807 \frac{m}{s^2}$$

$$F_{fin} := W_{fin} \cdot g = 9.611\,N$$

$$T_{fin} := F_{fin} \cdot L_{arm} = 1.057\,J$$

$$\rho_{water} := .001 \frac{kg}{cm^3}$$

$$A_{water} := 41in^2 = 264.516 \cdot cm^2$$

$$L_{water} := \frac{33.02}{2} cm$$

$$V_{water} := \sqrt{\frac{\left(2 \cdot \left|T_{fin}\right|\right)}{\left(\rho_{water} \cdot A_{water} \cdot L_{water}\right)}}$$

$$V_{water} = 0.696 \frac{m}{s}$$

Figure 25: Moment Arm Measurement System

4.2.3 Maximum allowable torque on the driveshaft

The maximum torque that the shaft could spin before failure was also tested to determine if the fin was a suitable design. With the fin removed from the masts, weights were added to the ends of the masts as seen in *Figure 26* below. The red circles indicate where the weights were added to the masts. Weight was added to the ends of the masts in 50 gram increments. The shaft worked properly up through 200 grams per mast. At 250 grams per mast the shaft the rockers are positioned on began to deflect a significant amount and the wheel used to turn the shaft began to slip and spin independent of the shaft. It was determined that 250 grams per mast was too much weight for this design to handle. Based on this experiment it was determined that the original fin design which weighed 1916 grams without the masts was too heavy and would provide too much torque. However, it was also determined that the new design of only one sheet of neoprene was

light enough to be moved by the shaft and that the problem with this fin was the shape of the fin and not the weight.

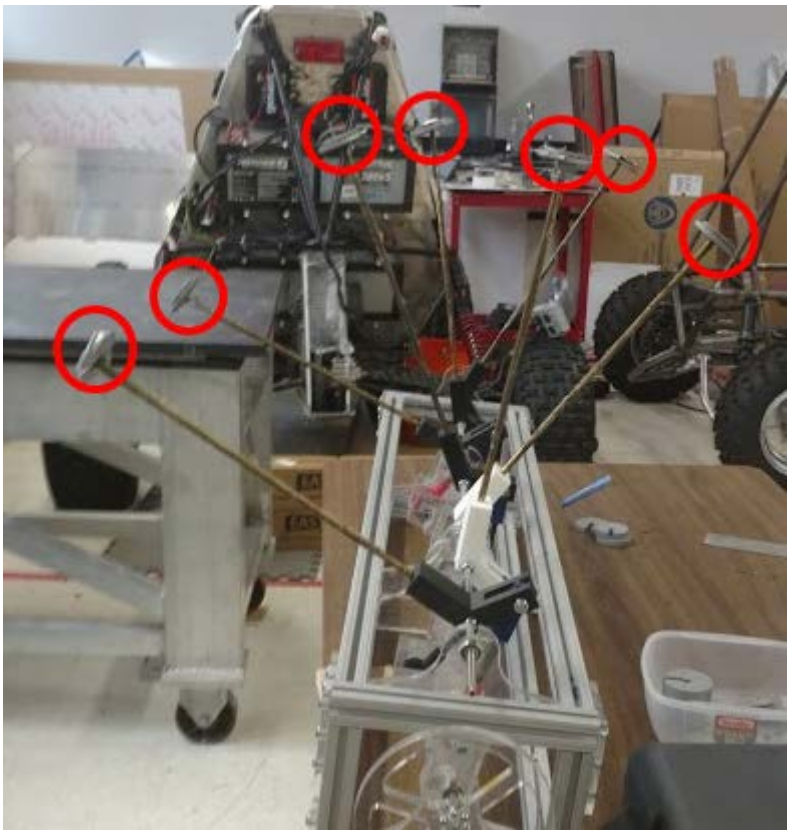

Figure 26: Maximum Loading Tests

4.3 Ansys

In order to better understand the effectiveness of the fin, we modelled the system in Ansys. In these tests, for the purposes of simplicity, we used a laminar flow model in concert with a constant pressure estimation. The fin's geometry was directly imported from SolidWorks, and used to create a mesh for simulation. The fin was then placed in a flow simulation, where iterations were run until the residuals stabilized. The result is pictured below in *Figure 27*.

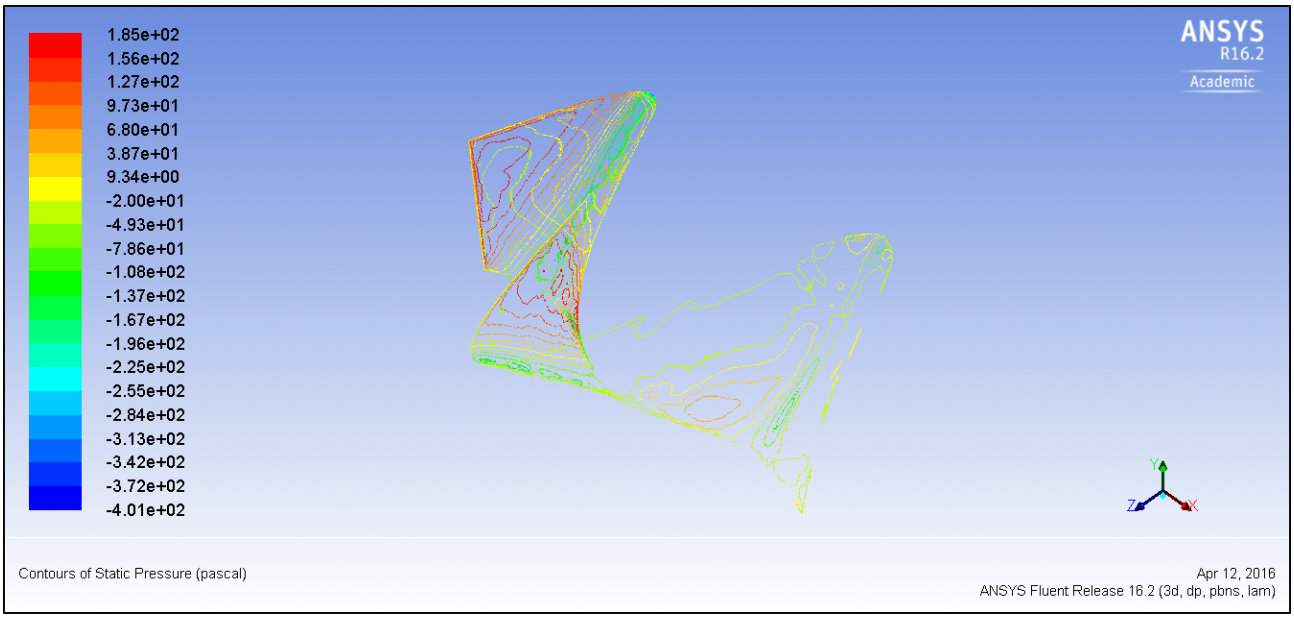

Figure 27: Ansys Simulation of Fin Model

In this simulation, the water flowed from the front to the back of the fin in the positive X direction. Based on this simulation, it is clear that the majority of the pressure exerted on the fin was generated in the first sine wave out the 1.5 sine waves present. This means that rear two rods and rear third of the fin were largely useless. A future design would be cognizant of this and design to these limitations. Because the design had the extra fin, it limited its effectiveness.

5. Redesign

5.1 Crankshaft

Between the two drivetrain designs, the crankshaft was determined to be more desirable in terms of simplicity and performance: however, several areas in this design should be subject to design changes if future iterations are pursued. The acrylic of the crankshaft made overall assembly difficult because special acrylic glue and intricate bolting was needed to ensure the web-journal subassemblies did not rotate about their positions. Pursuing a different material like aluminum will make assembly more precise and avoid potential for slip if paired with suitable bonding methods like welding. Having a single-piece crankshaft prevents the drivetrain from rotating about itself. The new material may also increase the weight of the driveshaft, therefore hollow or thin-walled stock should also be explored. Because the crankshaft designed used solid blocks of acrylic, some material may have been unnecessary and extraneous to its function. The thickness of the webs was designed to match the length of the frame. However, the length of the webs can compensate for reduction in web thickness. Overall, the most important design change is to use a different material for the crankshaft as it affects the ease of assembly and reliability.

It is advised in the future that a crankshaft should not be manufactured on campus for a similar project unless the project team has the budget and skills necessary to produce a solid crankshaft with no fasteners incorporated. Otherwise, a custom-ordered crankshaft is a better, though less cost-efficient, option.

5.2 Camshaft

Due to time constraints, the crankshaft was the only drivetrain tested both by bench testing and pool testing. The camshaft, however, could still be considered as a feasible design for the drivetrain. Slight modifications to the camshaft would be needed to ensure the mechanism would be successful in its purpose. Due to the many iterations of the camshaft, it was difficult to determine the ideal diameters for the inner circles of the cam. Without determining the correct diameter for the cam, friction points occurred on the shaft increasing the losses of the overall device. Therefore slight changes to the diameters will be necessary for smoother motion of the camshaft. This will also include the consideration of tolerancing for the laser cutter when cutting

the acrylic used as the laser cutter does not cut with zero thickness and creates a draft angle while cutting.

For the redesign of the camshaft, a bearing should also be purchased. The team had originally manufactured the bearings for the cams using 0.25 inch ball bearing. This lead to a difficulty in manufacturing as the balls would not always remain in the acrylic rings. Purchasing bearings would reduce the time spent on assembly and reduce the losses of the camshaft.

A square shaft should be used instead of a hexagonal shaft as the drivetrain. The individual cams will need to be 90 degrees offset from one another and a square shaft will ensure more accurate positioning of these cams. It will also be easier to attach the cams to the drivetrain if a square shaft is used. The set screws would slip into a different orientation which was perpendicular to a flat face on the hex shaft which changed the angles of alignment between the cams so they were no longer 90 degrees. With a square shaft, there would be no slippage as they would already be perpendicular to the face of the shaft.

5.3 Fin

Based on the Ansys simulations, the fin should be designed to incorporate only one sine wave of motion. The simulation clearly demonstrates that vast majority of the pressure needed to generate power is applied to the first sine wave of the existing fin. The extra weight of the fins and masts that provided the last 0.5 sine waves resulted in additional torque required to spin the shaft without greatly adding to the power output of the system. A future iteration should take advantage of this by removing the excess weight to maximize performance.

Another way of improving performance would be to use a different material for the fin. While the neoprene did demonstrate many of the properties needed for a successful fin, such as water resistance and the appropriate flexibility, it has a relatively high density among polymers. The high density results in a high fin weight which makes the starting torque of the system higher. Replacing the neoprene with a less dense material would lower the starting torque of the system, as well as the losses of power to the weight of the fin. One suggestion would be to research a synthetic fabric, such as waterproof canvas, or another thin, water-impermeable fabric. This would achieve the desired functionality while still being light enough to require less force to turn the shaft.

Changing the shape of the fin would also greatly improve the design. The fin design for this project had to have slits cut down a portion of the radius of the fin to allow for better movement of the masts. This was due to the fact that the fin was restricting the distance between the masts providing tension in the system. Increasing the arc length of the top arc of the fin would remove the need to cut slits in the fin once again allowing the fin to be a solid continuous piece.

5.4 Gearbox and Motor

The direct output from the fin was designed to be low velocity with high torque mechanical power. To effectively convert this power into electrical energy, the output must be reduced into high velocity, low torque power. A gearbox connected between the driveshaft and the induction motor shaft to properly reduce the power.

From the previous energy harvester, the maximum shaft speed was observed to be 35 RPM for the hybrid fin while the maximum was 25 RPM for the 30.5 cm neoprene fin. The maximum observed torque was 3 N*m and 3.6 N*m respectively. The minimum speeds were 1.5 RPM and 1 RPM. Using the fundamental laws of gearing, the gear ratio may be calculated (Norton, 2012).

The driving parameter is the expected range of speeds at which the motor will generate electricity. This value was determined by the electrical group to be at least 1000 RPM for their chosen motor. This determined the ratio to be in the area of 60:1, a very difficult gearing ratio to accomplish with the losses that will happen in the gearbox. With this gearing ratio it is suggested that the gearbox consist of several gears that gradually change diameter to reduce the amount of slippage in the gears. A suitable gear box will likely be comprised of a gear train that is composed of spur gears. This would allow incremental gearing, which would help reduce the losses in the system. Another mechanism might be a constantly variable transmission, which allows for continuous changing of the gear ratio. A continuously changing ratio can also be helpful to maximizing power output.

Based on these gearing ratios it is recommended that a motor with a lower RPM range be chosen to reduce the need for such a high gearing ratio. Alternatively, increasing the scale of the design so it can be run at higher RPM ranges that are closer to that of the motor could help performance.

6. Conclusions

There is an increasing demand to find new clean energy sources due to a rising demand for power. A developing sector of clean energy that as of yet has very few cost efficient power generating systems is tidal energy. Tidal turbines are currently inefficient and not popular in the clean energy sector. This project provides some insight into a potentially more feasible and efficient design. Instead of horizontally positioned fins that rotate in the flow of the water, our design is comprised of a fin that is oriented with the current, similarly to an eel's dorsal fin.

The Water Energy Harvester project is a continuation of a previous MQP which initialized the basic design for a tidal turbine. This project worked to improve the fin and drivetrain in pursuit of a more power-efficient, and manufacturable design. The fin was redesigned to use seven masts to generate 1.5 sine waves of motion. A camshaft was created to allow for direct comparison of results from the previous MQP. The crankshaft was created to explore the drivetrain concept and to attempt to increase power output from the device.

When building the device, the team ran into several setbacks. The first was the feasibility of manufacturing a crankshaft on WPI's campus. It quickly became apparent that manufacturing a crankshaft out of acrylic would not be successful and would require custom manufacturing of a metal that would not be feasible on WPI's campus. Pool testing did not yield the data necessary to prove the design concept due to inadequacies in the bonding of the crankshaft. It did yield a cut in speed of approximately 0.75 m/s. Bench testing resulted in the minimum torque necessary to spin the shaft which can be used to calculate minimum flow velocity. The maximum torque was also calculated from bench testing. Based on bench testing the cut in speeds was determined to be 0.696 m/s. Due to setbacks that the team faced, quantitative results were not collected, and most of the time spent was used trying to modify the design in order to produce a working prototype. If this project is to be continued in the future it is recommended that the design of the camshaft, crankshaft, fin, gearing and motor be revised to create a working model which provides more solid results.

References

Blevins, E. L., & Lauder, G. V. (2012). Rajiform locomotion: three-dimensional kinematics of the pectoral fin surface during swimming in the freshwater stingray Potamotrygon orbignyi. Journal of Experimental Biology.

Boileau, R., Fan, L., & Moore, T. (2002). Mechanization of Rajiform Swimming Motion. The making of Robo Ray.

Choucri, N. (2012). Renewable Energy Technologies: Cost Analysis Series, Hydropower. Volume 1: Power Sector. Energy and Development: Fossil Fuels in Developing Countries. Energy for Survival and Development(57).

Costanzo, I., Kelsey, A., Ogren, F., Wians, D. (2015) Design of a Novel Concept for Harnessing Tidal Stream Power. Major Qualifying Project, Worcester Polytechnic Institute.

DTI. (2002) Engineering Business: Research and Development of a 150 kw Tidal Stream Generator - Phase 1. Retrieved from http://www.dti.gov.uk/renewables/publications/pdfs/T00211.pdf

DTI. (2003) Engineering Business: Research and Development of a 150 kw Tidal Stream Generator - Phase 2. Retrieved from http://www.dti.gov.uk/renewables/publications/pdfs/T00211.pdf

DTI. (2005) Engineering Business: Stingray Tidal Stream Energy Device Phase 3. Retrieved from http://www.dti.gov.uk/renewables/publications/pdfs/T00211.pdf

Environmental Impacts of Hydroelectric Power. (2015). Union of Concerned Scientists.

Epstein, M., Colgate, J. E., & MacIver, M. A. (2006). Generating thrust with a biologically-inspired robotic ribbon fin. 2412-2417.

Friedel, Robert. (2007). A Culture of Improvement: Technology and the Western Millennium

Friction and Coefficients of Friction. (2016). Retrieved from http://www.engineeringtoolbox.com/friction-coefficients-d_778.html

Herrel, A., Choi, H., De Schepper, N., Aerts, P., & Adriaens, D. (2011). Kinematics of swimming in two burrowing anguilliform fishes. Zoology, 114(2), 78-84.

How Geothermal Energy Works. (2015). Union of Concerned Scientists.

How Solar Energy Works. (2015). Union of Concerned Scientists.

International Energy Agency, & Electronic Journals Library. (1998). Key world energy statistics from the IEA. Key World Energy Statistics from the IEA

Key World Energy Statistics. (2014). Retrieved: http://www.iea.org/publications/freepublications/publication/KeyWorld2014.pdf

Lauder, G. V., & Drucker, E. G. (2004). Morphology and experimental hydrodynamics of fish fin control surfaces. IEEE Journal of Oceanic Engineering, 29(3), 556-571.

McMaster-Carr. (2015). Retrieved from http://www.mcmaster.com/

Murray, Peter. (2012) First Offshore Turbine For U.S. Begins Feeding Power To Maine's Grid. Retrieved from http://singularityhub.com/2012/11/01/first-offshore-turbine-for-u-s-begins-feeding-power-to-maines-grid/

Navigant Consulting, Inc. (2009). Job Creation Opportunities in Hydropower. Retrieved from http://www.hydro.org/wp-content/uploads/2010/12/NHA_JobsStudy_FinalReport.pdf

NREL (2015). Levelized Cost of Energy Calculator. Retrieved: http://www.nrel.gov/analysis/tech_lcoe.html

Niu, X., Xu, J., Ren, Q., & Wang, Q. (2014). Locomotion learning for an anguilliform robotic fish using central pattern generator approach. IEEE Transactions on Industrial Electronics, 61(9), 4780-4787.

Norton, R. L. (2012). Design of machinery: An introduction to the synthesis and analysis of mechanisms and machines (5th ed.). New York: McGraw-Hill.

Prono, L. (2012). Alliance to Save Energy. In S. G. Philander (Ed.), Encyclopedia of Global Warming & Climate Change (2nd ed., Vol. 1, pp. 36-38). Thousand Oaks, CA.

Rosenberger, L. J. (2001). Pectoral fin locomotion in batoid fishes: undulation versus oscillation. Journal of Experimental Biology.

Singh, Timon. (2012) Maine Launches the First Commercial Tidal Power Project in the US!. Retrieved from http://inhabitat.com/maine-launches-the-first-commercial-tidal-power-project-in-the-us/

Thompson, Ross. (2009). Structures of Change in the Mechanical Age: Technological Invention in the United States

Types of Renewable Energy: A Cost Comparison. (2015). Green Electricity Guide

U. N. D.P. (2000). World Energy Assessment - Energy and the Challenge of Sustainability. Retrieved from http://www.undp.org/content/dam/aplaws/publication/en/publications/environment-energy/www-ee-library/sustainable-energy/world-energy-assessment-energy-and-the-challenge-of-sustainability/World%20Energy%20Assessment-2000.pdf

U.S. Energy Information Administration (EIA). (2015). Future world energy demand driven by trends in developing countries. Today in Energy. Retrieved from http://www.eia.gov/todayinenergy/detail.cfm?id=14011

US EPA. (2015). Energy and the Environment.

US EPA. (2015). Future Climate Change.

US EPA. (2015). U.S. Greenhouse Gas Inventory Report.

Wikander, Örjan. (1999). Handbook of Ancient Water Technology

William S. Vorus Brandon M. Taravella. (2011). Anguilliform fish propulsion of highest hydrodynamic efficiency. Journal of Marine Science and Application, 10(2), 163-174.

Wind and Solar Energy. (2015). Retrieved from http://www.cleanlineenergy.com/technology/wind-and-solar

World Nuclear Association (2011). Comparison of Lifecycle Greenhouse Gas Emissions of Various Electricity Generation Sources. Retrieved from http://www.world-nuclear.org/uploadedFiles/org/WNA/Publications/Working_Group_Reports/comparison_of_lifecycle.pdf

Woody, T. (2015). Here's Why Developing Countries Will Consume 65% of the World's Energy by 2040.

Appendices

Appendix A: Fin Dimensions

$len := 30$

$x := 0, 0.01 .. len$

$n := 5$

$$\lambda := 360 \cdot \frac{\left(\frac{30}{7}\right)}{15 \cdot n}$$

$\lambda = 20.571$

$rtip := 13$

$rbase := 1$

$$\theta max := 45 \frac{\pi}{180}$$

$$form(x) := \theta max \cdot \sin\left(2\pi \frac{x}{\lambda}\right)$$

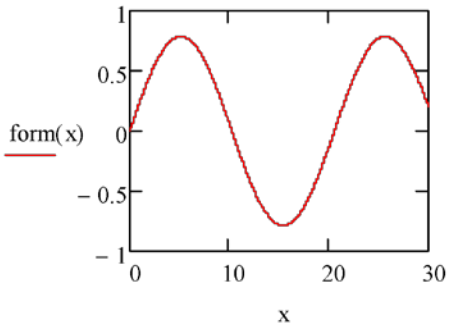

$$edgeL(r) := \int_0^{len} \sqrt{1 + \left[\frac{d}{dl}((form(l) \cdot r))\right]^2}\, dl$$

$Ltip := edgeL(rtip) = 67.937$

$Lbase := edgeL(rbase) = 30.415$

$$r1 := Lbase \cdot \frac{(rtip - rbase)}{(Ltip - Lbase)} = 9.727$$

$r2 := rtip - rbase + r1 = 21.727$

$$\theta := \frac{Lbase}{r1} = 3.127$$

$$\theta := \frac{Ltip}{r2} = 3.127$$

$$3.127 \cdot \frac{180}{\pi} = 179.164$$

Appendix B: FEA Program Results

Program Set Up:

The fin and mast assembly was first created in SolidWorks. All surfaces were then joined to create a single solid body. This was then exported as a parasolid file (.x_t file extension) to be used in Ansys. A second identical copy was made, with the exception of a large, thin disk placed in front of the fin to be used as a flow generation source. This was also exported as a parasolid. The flow was set to 2 m/s, the maximum velocity expected during testing. The fin and disk were imported as a geometry (A), then meshed using a CFD mesh optimized for Fluent (B), which was then imported into a Fluent CFD solver (D). The materials for the fin and the various mast types were assigned in an engineering data library (C). The solution of the Fluent analysis was then imported into a structural analysis (D), which produced the stress estimates desired. An image of this schematic is below. Fluent was used to model the expected forces on the fin as it moved through the water. The boundary conditions were set to be a constant 2 m/s flow and generated from a source large enough to avoid potentially confounding results from boundary interactions with the fin. This result was fed into a structural analysis which then determined which materials would be outside of their operational range for our application.

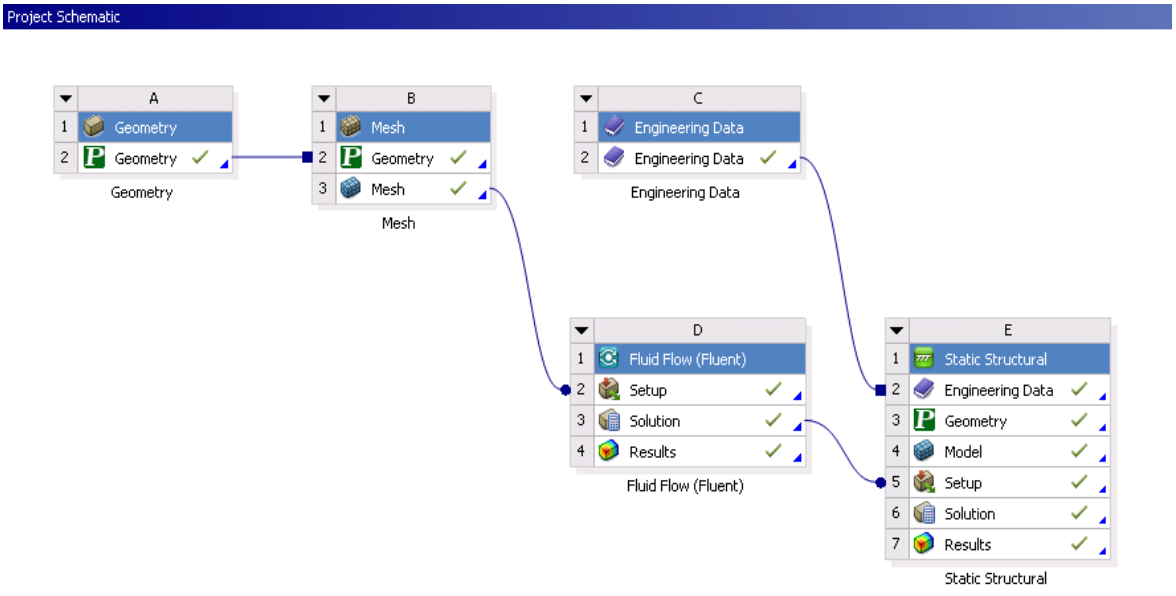

Figure 18: Ansys Simulation Setup

Results for different materials are pictured below.

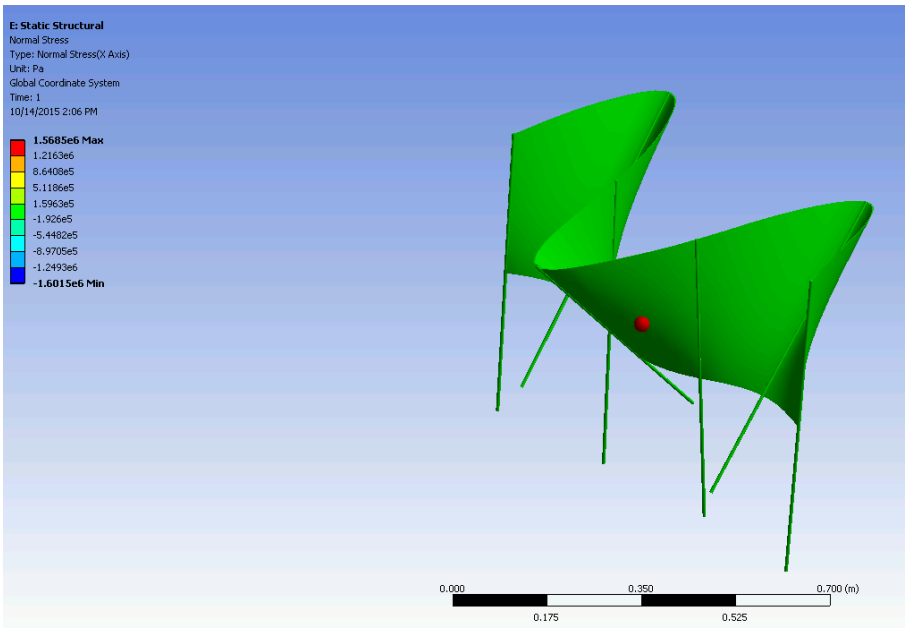

Figure 28: Normal Stress on Aluminum Masts

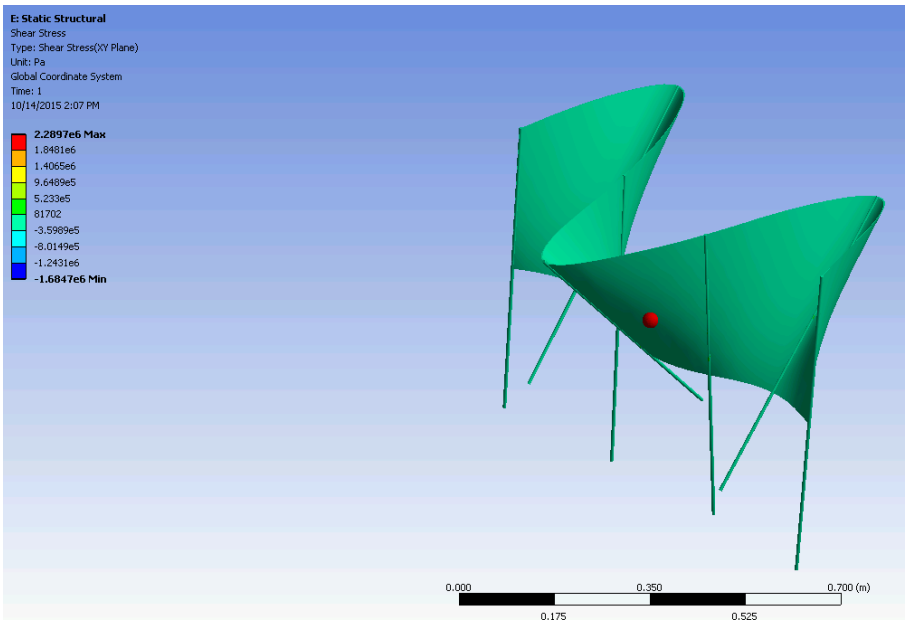

Figure 29: Shear Stress on Aluminum Masts

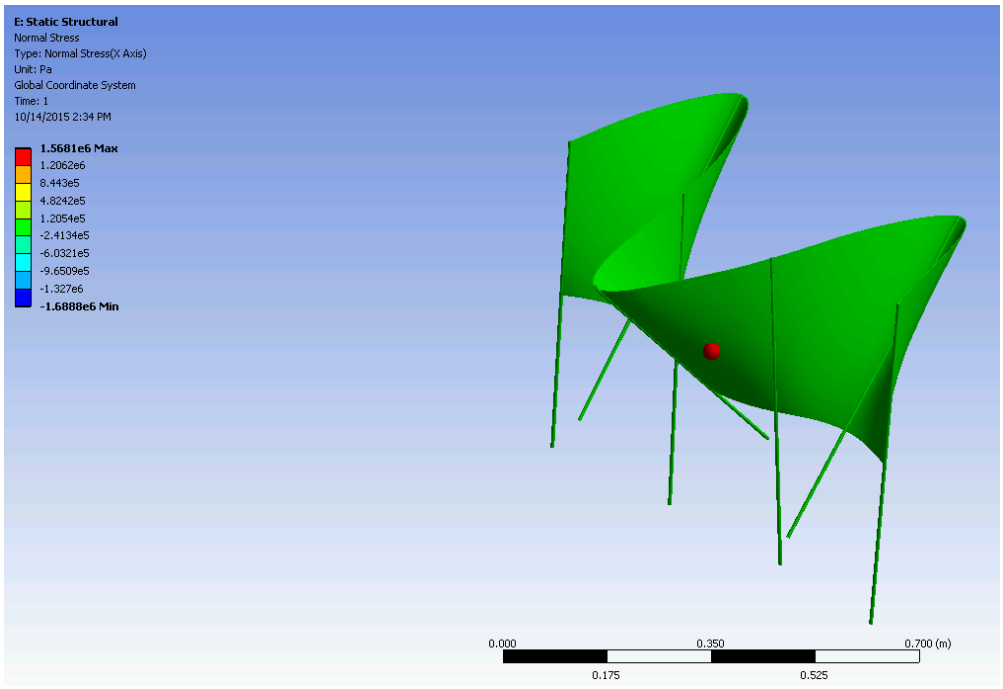

Figure 30: Normal Stress on Brass Masts

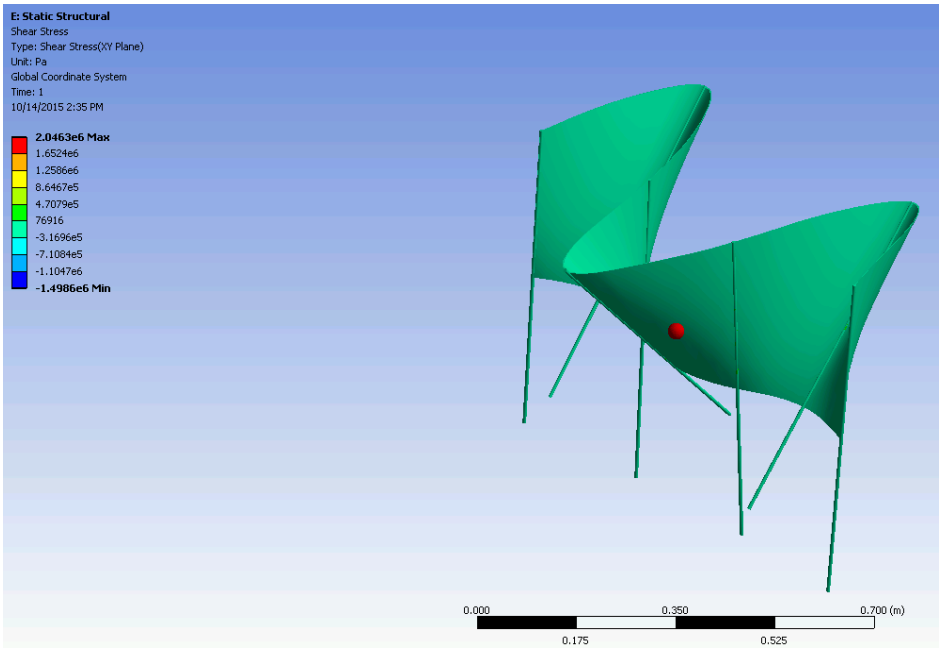

Figure 31: Shear Stress on Brass Masts

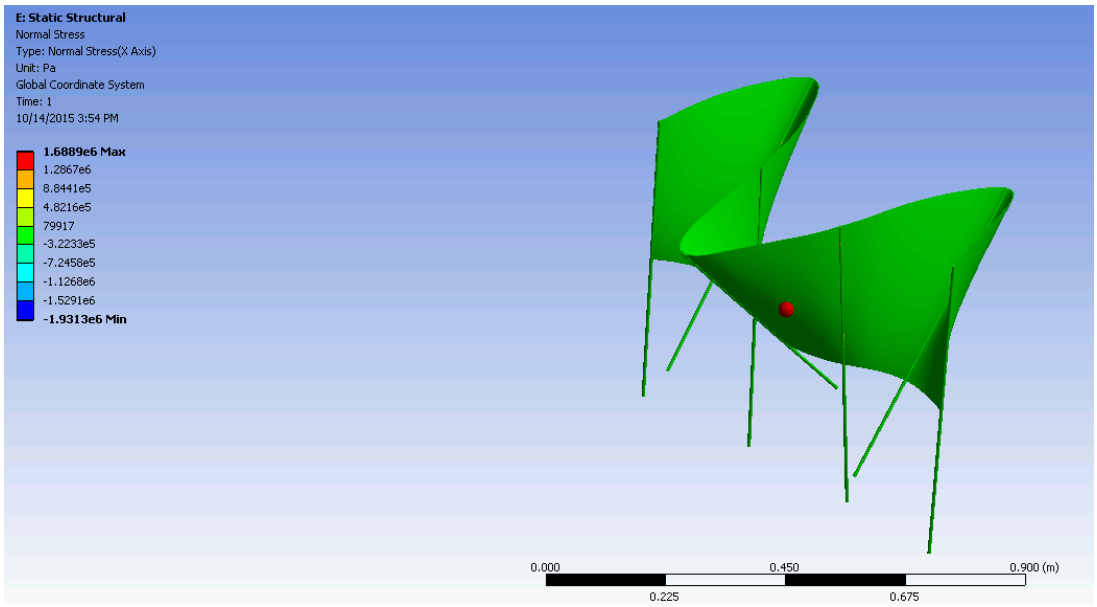

Figure 32: Normal Stress on Stainless Steel Masts

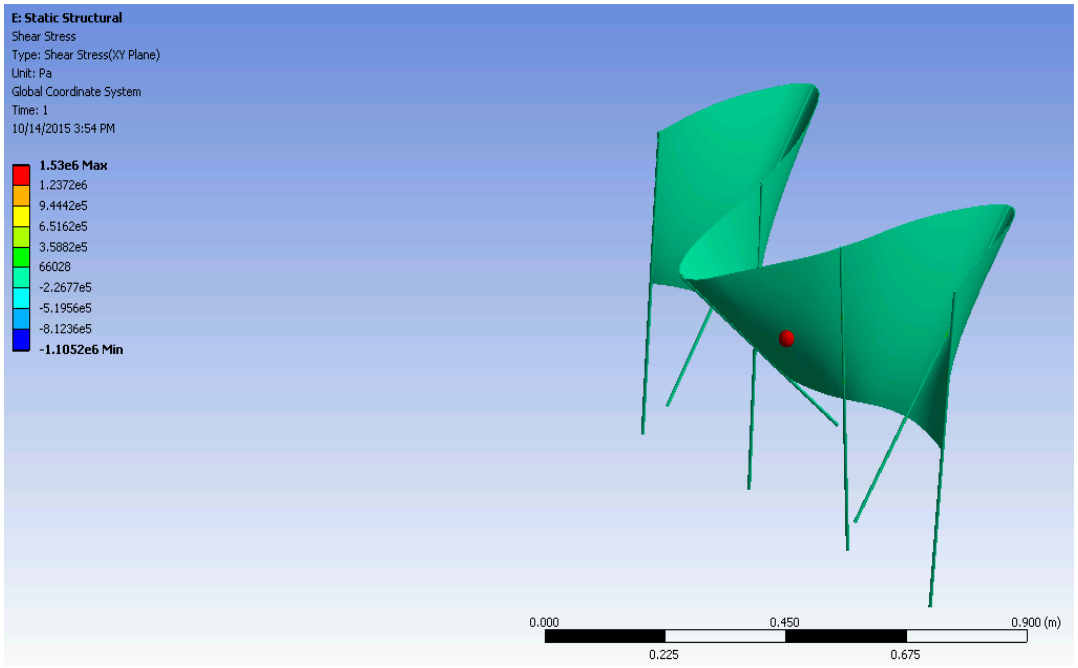

Figure 33: Shear Stress on Stainless Steel Masts

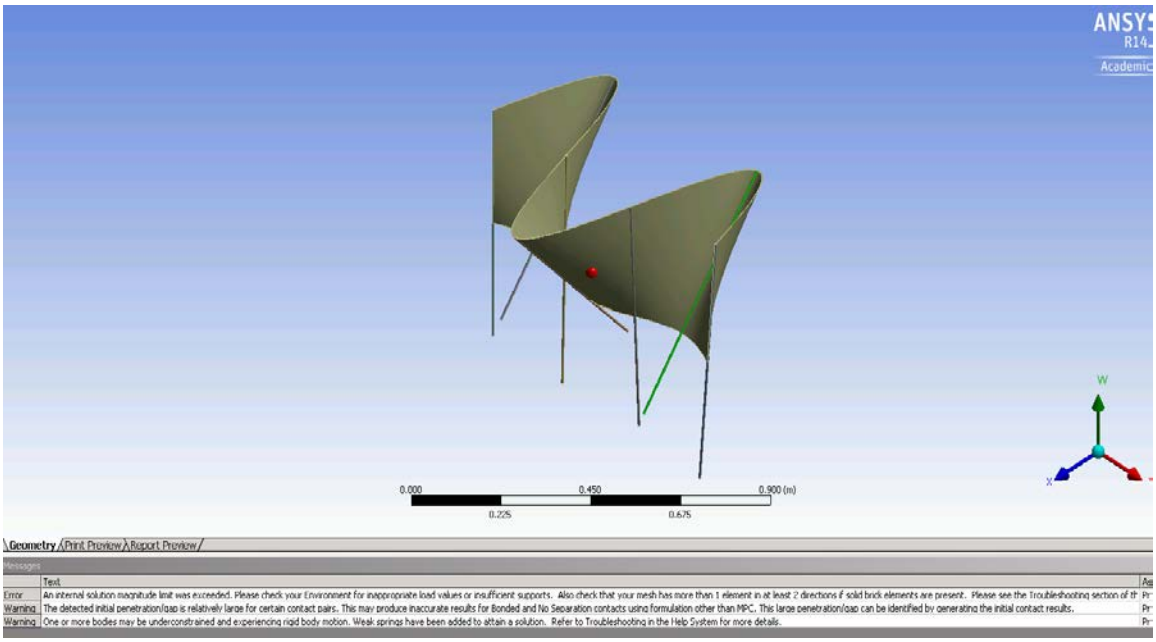

Figure 34: Failed Nylon Masts

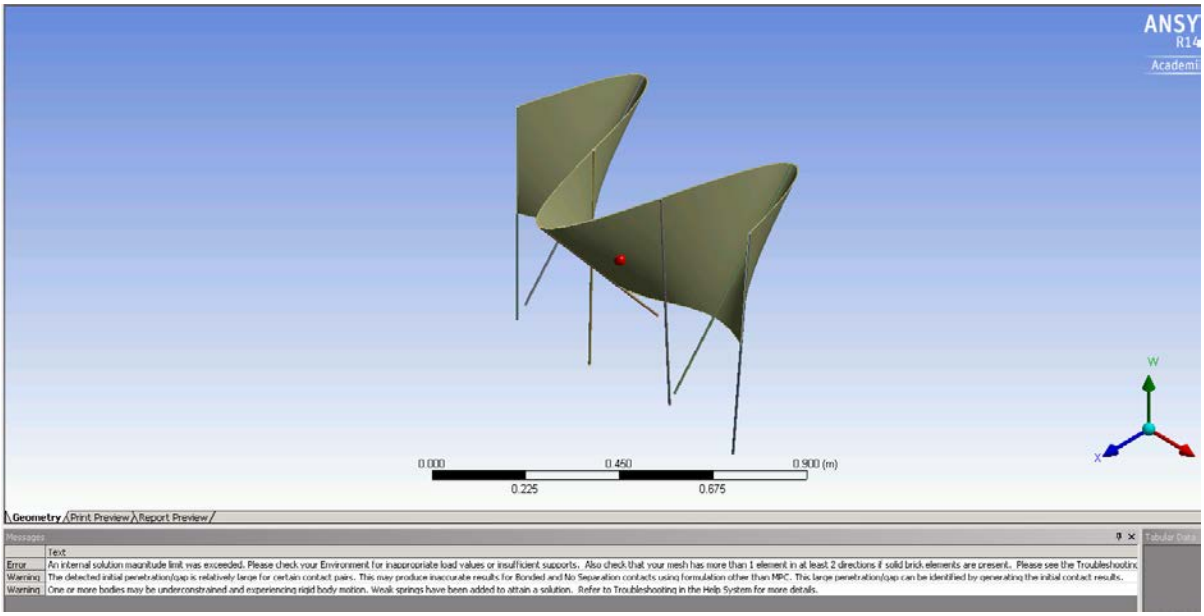

Figure 35: Failed Polycarbonate Masts

Appendix C: Torque Calculations

$\rho_{brass} := .00855 \frac{kg}{cm^3}$

$\rho_{water} := .001 \frac{kg}{cm^3}$

$W_{fin} := .958kg$

$g = 9.807 \frac{m}{s^2}$

$L_{fin} := \frac{33.02}{2} cm$

$L_{water} := \frac{33.02}{2} cm$

$D_{mast} := .635cm$

$L_{mast} := 33.02cm$

$A_{water} := 41in^2 = 264.516 \cdot cm^2$

The weight of one mast needs to be calculated using the density as this weight is not included in the weight of the neoprene fin

$W_{mast} := \rho_{brass} \cdot D_{mast}^2 \cdot \frac{\pi}{4} \cdot L_{mast} = 0.089kg$

The torque for each mast is calculated using the weight of the mast and 1/7 the weight of the fin, as there are 7 masts. Three different positions of the fin were calculated.

The first position of the fin

$$T_{fin1} := g \cdot \left(\frac{W_{fin}}{7} + W_{mast} \right) \cdot L_{fin} \cdot \cos\left(\frac{\pi}{4} \right) = 0.259 \cdot N \cdot m$$

$$T_{fin2} := g \cdot \left(\frac{W_{fin}}{7} + W_{mast} \right) \cdot L_{fin} \cdot \cos\left(\frac{\pi}{2} \right) = 0 \cdot N \cdot m$$

$$T_{fin3} := g \cdot \left(\frac{W_{fin}}{7} + W_{mast} \right) \cdot L_{fin} \cdot \cos\left(\frac{\pi}{2} \right) = 0 \cdot N \cdot m$$

$$T_{fin4} := g \cdot \left(\frac{W_{fin}}{7} + W_{mast} \right) \cdot L_{fin} \cdot \cos\left(\frac{\pi}{2} \right) = 0 \cdot N \cdot m$$

$$T_{fin5} := g \cdot \left(\frac{W_{fin}}{7} + W_{mast} \right) \cdot L_{fin} \cdot \cos\left(\frac{\pi}{2} \right) = 0 \cdot N \cdot m$$

$$T_{fin6} := g \cdot \left(\frac{W_{fin}}{7} + W_{mast} \right) \cdot L_{fin} \cdot \cos\left(\frac{3\pi}{4} \right) = -0.259 \cdot N \cdot m$$

$$T_{fin7} := g \cdot \left(\frac{W_{fin}}{7} + W_{mast} \right) \cdot L_{fin} \cdot \cos\left(\frac{3\pi}{4} \right) = -0.259 \cdot N \cdot m$$

Fin in a second position

$$T_{fin8} := g\cdot\left(\frac{W_{fin}}{7} + W_{mast}\right)\cdot L_{fin}\cdot\cos\left(\frac{\pi}{4}\right) = 0.259\cdot N\cdot m$$

$$T_{fin9} := g\cdot\left(\frac{W_{fin}}{7} + W_{mast}\right)\cdot L_{fin}\cdot\cos\left(\frac{\pi}{4}\right) = 0.259\cdot N\cdot m$$

$$T_{fin10} := g\cdot\left(\frac{W_{fin}}{7} + W_{mast}\right)\cdot L_{fin}\cdot\cos\left(\frac{\pi}{2}\right) = 0\cdot N\cdot m$$

$$T_{fin11} := g\cdot\left(\frac{W_{fin}}{7} + W_{mast}\right)\cdot L_{fin}\cdot\cos\left(\frac{\pi}{2}\right) = 0\cdot N\cdot m$$

$$T_{fin12} := g\cdot\left(\frac{W_{fin}}{7} + W_{mast}\right)\cdot L_{fin}\cdot\cos\left(\frac{\pi}{2}\right) = 0\cdot N\cdot m$$

$$T_{fin13} := g\cdot\left(\frac{W_{fin}}{7} + W_{mast}\right)\cdot L_{fin}\cdot\cos\left(\frac{3\pi}{4}\right) = -0.259\cdot N\cdot m$$

$$T_{fin14} := g\cdot\left(\frac{W_{fin}}{7} + W_{mast}\right)\cdot L_{fin}\cdot\cos\left(\frac{3\pi}{4}\right) = -0.259\cdot N\cdot m$$

The third position of the fin

$$T_{fin15} := g\cdot\left(\frac{W_{fin}}{7} + W_{mast}\right)\cdot L_{fin}\cdot\cos(1.178097) = 0.14\cdot N\cdot m$$

$$T_{fin16} := g\cdot\left(\frac{W_{fin}}{7} + W_{mast}\right)\cdot L_{fin}\cdot\cos(1.178097) = 0.14\cdot N\cdot m$$

$$T_{fin17} := g\cdot\left(\frac{W_{fin}}{7} + W_{mast}\right)\cdot L_{fin}\cdot\cos(1.9634955) = -0.14\cdot N\cdot m$$

$$T_{fin18} := g\cdot\left(\frac{W_{fin}}{7} + W_{mast}\right)\cdot L_{fin}\cdot\cos(1.9634955) = -0.14\cdot N\cdot m$$

$$T_{fin19} := g\cdot\left(\frac{W_{fin}}{7} + W_{mast}\right)\cdot L_{fin}\cdot\cos(1.178097) = 0.14\cdot N\cdot m$$

$$T_{fin20} := g\cdot\left(\frac{W_{fin}}{7} + W_{mast}\right)\cdot L_{fin}\cdot\cos(1.178097) = 0.14\cdot N\cdot m$$

$$T_{fin21} := g\cdot\left(\frac{W_{fin}}{7} + W_{mast}\right)\cdot L_{fin}\cdot\cos(1.9634955) = -0.14\cdot N\cdot m$$

With 4 of the masts at a 90 degree angle, one mast at 45 degrees and two mast at 135 degrees the torques will add up to be -0.259 N*m

$$T_1 := T_{fin1} + T_{fin2} + T_{fin3} + T_{fin4} + T_{fin5} + T_{fin6} + T_{fin7} = -0.259\cdot N\cdot m$$

With 3 of the masts at a 90 degree angle, two masts at 45 degrees and two masts at 135 degrees the torques will add up to be 0 N*m

$$T_2 := T_{fin8} + T_{fin9} + T_{fin10} + T_{fin11} + T_{fin12} + T_{fin13} + T_{fin14} = 0\cdot N\cdot m$$

With 4 of the masts at a 67.5 degree angle, three masts at a 112.5 degree angle the torques will add up to be 0.14 N*m

$$T_3 := T_{fin15} + T_{fin16} + T_{fin17} + T_{fin18} + T_{fin19} + T_{fin20} + T_{fin21} = 0.14\cdot N\cdot m$$

From this torque the minimum theoretical flow velocity of water can be calculated. The flow velocity will need to be higher than this due to losses due to friction and inefficiencies in the design

$$T_{water} := \rho_{water} \cdot A_{water} \cdot \frac{1}{2} \cdot V^2 \cdot L_{water}$$

$$V_1 := \sqrt{\frac{2(|T_1|)}{(\rho_{water} \cdot A_{water} \cdot L_{water})}}$$

$$V_1 = 0.344 \frac{m}{s}$$

$$V_2 := \sqrt{\frac{2(T_2)}{(\rho_{water} \cdot A_{water} \cdot L_{water})}}$$

$$V_2 = 7.131 \times 10^{-9} \frac{m}{s}$$

$$V_3 := \sqrt{\frac{2(T_3)}{(\rho_{water} \cdot A_{water} \cdot L_{water})}}$$

$$V_3 = 0.253 \frac{m}{s}$$

For the cut in speed experimentally determined to be .75 m/s the torque that the water provides can be calculated.

$$V_{water} := .75 \frac{m}{s}$$

$$T_{Water} := \rho_{water} \cdot A_{water} \cdot \frac{1}{2} \cdot \left(.75 \frac{m}{s}\right)^2 \cdot L_{water} = 1.228 \cdot N \cdot m$$

Using the minimum torque from the moment arm tests the cut in speed was calculated.

$$V_{Water} := \sqrt{\frac{2(|1.057 N \cdot m|)}{(\rho_{water} \cdot A \cdot L_{water})}} = 0.113 \frac{m^2}{A^{0.5} \cdot s}$$

Because the cut in speed was only tested in increments of 0.25 m/s, it can be said that the experimental data proves the validity of the calculations for the cut in speed of the device